University of Nottingham
UK | CHINA | MALAYSIA

MRes Thesis

Optimisation of Delivery of the Ataxia Telangiectasia Mutated Transgene to HeLa Cells Using Glycosaminoglycan Enhanced Transduction

Student: Ala'a Siam

Main Supervisor: Dr James E Dixon

Date of Submission: 07/10/2021

Word Count: 26,001

Statements & Declarations

Declaration of Authorship:

I hereby declare that the research presented in this thesis is the result of my original work and has been written by me, except where specifically indicated in the text. Any assistance that I have received has been appropriately acknowledged, and any information sources I relied on are referenced. I declare that this thesis has not been submitted for a degree at any university aside from the University of Nottingham.

Ala'a Siam

07/10/2021



Statement on COVID-19 Impact:

The experimental component of this thesis has been significantly disrupted by the university's closure in response to the COVID-19 global pandemic. This closure prevented the conduction of several planned experiments. It also prevented the conduction of experimental repetitions that were necessary for several planned statistical analyses.

Abstract

Ataxia telangiectasia (AT) is a monogenic syndrome that is characterised by hypersensitivity to ionising irradiation. This study is part of a proof-of-concept project for a non-viral gene therapy that utilises glycosaminoglycan-enhanced transduction (GET), which is based on transfection peptides that fuse membrane docking and cell penetrating domains. Previous work has demonstrated delivery of plasmid DNA (pDNA) encoding the AT-mutated gene (ATM) *in vitro* using the GET peptides FLR and FLH. The aim of this study is to optimise the GET formulation *in vitro* for delivery and expression of ATM pDNA in HeLa cells. Attempts were made to capture transgene expression via *Zoanthus sp*. green fluorescent protein (zsGreen) fluorescence and immunostaining, and to visualise results by flow cytometry and confocal microscopy. Results suggest that transfection efficiency may positively correlate with peptide : pDNA mass ratio (PDMR). They also suggest that the proteosome inhibitor MG132 may better stabilise ATM expression than the histone deacetylase inhibitor suberanilohydroxamic acid (SAHA). These results were found by flow cytometry for zsGreen fluorescence. Microscopic results due to experimental factors were inconsistent with those of flow cytometry, whereas immunostaining analysis was precluded by nonspecific binding of the secondary antibody. Further optimisation requires reproducing results for statistical analysis, validating ATM expression by immunostaining and microscopy, and replicating transfection results in $ATM^{-/-}$ fibroblasts. Future directions include establishing functionality of transfected ATM using irradiation assays, exploring effects of genomic integration on ATM expression, and developing formulations for *in vivo* performance using animal models.

Acknowledgements

I acknowledge the extensive support of my main supervisor, Dr James Dixon. I acknowledge the support of Dr Joshua Branter, who played a key role in training me on the assays used in this project and oversaw my daily work in the lab during the initial stages of my MRes. I have received key training from Dr David Onion on flow cytometry, and from Mr Ian Ward on confocal microscopy. I also acknowledge the roles of Drs Catherine Jopling and Lisa White, who have provided me with extensive support regarding postgraduate study affairs. Primary and immortalised $ATM^{-/-}$ fibroblasts have been generously and respectively provided by Professor Malcolm Taylor of the University of Birmingham and Professor Ignacio J Molina of the University of Granada. I also acknowledge the roles of Professor Ronald Chalmers and Dr Stewart Martin, who have agreed to co-supervise the future directions of the project respectively in genome editing and functionality assays. I acknowledge the general support that I have received from the rest of the Dixon group, as well as from the staff of the School of Pharmacy and the Biodiscovery Institute at the University of Nottingham. Finally, I acknowledge the deep support I received from my family. I particularly value all these contributions given the extraordinary circumstances and significant disruptions caused by the COVID-19 pandemic.

Table of Contents

Statements & Declarations 2
Declaration of Authorship 2
Statement of COVID-19 Impact 2
Abstract 3
Acknowledgements 4
Table of Contents 5
Abbreviations 7
Tables & Figures 10
Tables 10
Figures 10
Chapter 1: Introduction 11
Section 1.1: Ataxia-Telangiectasia (AT) 12
Section 1.2: Molecular Biology of ATM 13
Section 1.3: Experimental Therapies for AT 16
Section 1.4: Experimental Models for AT Therapeutics 20
Section 1.5: Glycosaminoglycan-Enhanced Transduction 24
Section 1.6: Implementation of GET Gene Therapy 28
Section 1.7: Implementation of GET for ATM Delivery 33
Section 1.8: Aims & Objectives 37
Chapter 2: Materials & Methods 40
Section 2.1: Materials 41
Subsection 2.1.1: Plasmids 41
Subsection 2.1.2: Cell Lines 42
Subsection 2.1.3: Reagents 42
Section 2.2: Methods 44
Subsection 2.2.1: Cell Culture 44
Subsection 2.2.2: Transfection 44
Subsection 2.2.3: Microscopy Endpoint Analysis 45
Subsection 2.2.4: Microscopy Immunostaining 47
Subsection 2.2.5: Flow Cytometry Endpoint Analysis 47
Subsection 2.2.6: Flow Cytometry Immunostaining 48
Chapter 3: Results 49
Section 3.1: Optimisation of GET Peptide : pDNA Mass Ratio 50
Section 3.2: Optimisation of ATM Stabilisation Regimens 58
Section 3.3: Analysing Immunostaining by Flow Cytometry 63
Chapter 4: Discussion 72
Chapter 5: Conclusions & Future Directions 85
Section 5.1: Conclusions 86
Section 5.2: Short-Term Directions 88
Subsection 5.2.1: Cellular Functionality Assays 89

Subsection 5.2.2: Molecular Functionality Assays 90
Section 5.3: Long-Term Directions 91
Subsection 5.3.1: Optimisation of GET for Brain Delivery 92
Subsection 5.3.2: Optimisation of Sustainable Expression of ATM 93
Subsection 5.3.3: *In Vivo* Experimentation with GET/ATM Nanoparticles 94
Subsection 5.3.4: Alternative GET Approaches for AT Therapy 95
Section 5.4: Clinical Outlook of GET-Mediated AT Gene Therapy 97
References 100

Abbreviations

- γH2AX: Phosphorylated H2AX
- AAV: Adeno-associated viral vector
- AB/AM: Antibiotic antimycotic
- AT: Ataxia-telangiectasia
- ATM: Ataxia-telangiectasia-mutated gene
- BSA: Bovine serum albumin
- Cas9: CRISPR-associated protein 9
- CMV: Cytomegalovirus
- CMVp: Cytomegalovirus promoter
- CPP: Cell-penetrating peptide
- CRISPR: Clustered regularly interspaced short palindromic repeats
- CSF: Cerebrospinal fluid
- dCas9: Deactivated Cas9
- DDR: DNA damage response
- DMEM: Dulbecco's Modified Eagle Medium
- DSB: Double strand break
- EDTA: Ethylenediaminetetraacetic acid
- F: Flag tag with amino acid sequence DYKDDDDK
- FAT: FRAP-ATM-TRRAP domain
- FATC: FAT carboxy-terminal domain
- FCS: Foetal calf serum
- GET: Glycosaminoglycan-enhanced transduction
- Glux: *G. princeps* luciferase

- gRNA: Guide RNA
- H: Poly-histidine tag
- HDR: Homology-directed repair
- HEAT: Huntington-elongation factor 3 protein phosphatase 2A-TOR1 domain
- hEF1A: Human elongation factor 1-α
- HFF: Human foreskin fibroblast
- HSC: Haematopoietic stem cell
- HSV: Herpes-simplex virus
- IV: Intravenous
- LV: Lentiviral vector
- MDP: Membrane-docking peptide
- MEth: 100% Methanol
- MiniATM: Truncated ATM gene corresponding to the spliced variant of EryDex®
- MRN: Mre11-Rad50-Nbs1 complex
- mRNA: Messenger RNA
- MSD: Mean square displacement
- MW: Molecular weight
- MyoD: Myogenic differentiation master regulator
- N: Sample size
- NADPH : Nicotinamide adenine dinucleotide phosphate
- NHEJ: Non-homologous end joining
- NLS: Nuclear localisation sequence
- p-ATM: Phosphorylated ATM
- p-p53: Phosphorylated p53

- P/S: Penicillin and Streptomycin
- PBS: Phosphate-buffered saline
- PBST: PBS with 0.1% Tween®20
- pCMV: Plasmid pCMV
- PCR: Polymerase chain reaction
- PDMR: GET peptide to pDNA mass ratio
- pDNA: Plasmid DNA
- PE: Plating efficiency
- PEG: Polyethylene glycol
- PFA: 4% Paraformaldehyde
- pGM: Plasmid pGM
- PI3K: phosphatidylinositol 3-kinase
- PIKK: PI3K-like protein kinases
- PLGA: poly (lactic-co-glycolic acid)
- PTM: Posttranslational modification
- RT-PCR: Reverse transcription polymerase chain reaction
- RUNX2: Runt-related transcription factor 2
- SAHA: Suberanilohydroxamic acid
- SF: Surviving fraction
- SSB: Single strand break
- SV40: Simian virus 40
- T2A: Self-cleaving peptide with sequence GSGEGRGSLLTCGDVEENPGP
- TTT: Tel2-Tti1-Tti2 complex
- zsGreen: *Zoanthus* sp. green fluorescent protein

Tables & Figures

Tables:

Table [1]: Nomenclature of Transfection Constructs 42
Table [2]: Quantitative Equivalences of Peptide Masses Employed for Transfection 46
Table [3]: Quantitative Analysis of pDNA Stocks 46
Table [4]: Compositions of Elevated PDMR Formulations 51
Table [5]: Transection Efficiencies with PDMR Elevation 51
Table [6]: Transfection Efficiencies with 5μM MG132 and/or 10μM SAHA Treatment 59

Figures:

Figure [1]: Structure of ATM 14
Figure [2]: Protein Fusion via Self-Cleaving Peptides 24
Figure [3]: Structures of GET Peptides and Nanoparticles 27
Figure [4]: Structures of pGM169 and pCMV-GFP 31
Figure [5]: Backbone Structures of Plasmids pGM and pCMV 41
Figure [6]: Structures of Transgenes Employed in this Study 43
Figure [7]: Transection Efficiency vs PDMR Plot 52
Figure [8]: Flow Cytometry Analysis for PDMR Elevation 56
Figure [9]: Transection Efficiency vs Treatment Regimen Plot 59
Figure [10]: Flow Cytometry Analysis for 5μM MG132 and/or 10μM SAHA Treatment 62
Figure [11]: Microscopic Analysis for 5μM MG132 Treatment 64
Figure [12]: Microscopic Evidence for Non-Specific Binding of Secondary Antibody 66
Figure [13]: Flow Cytometry Analysis for 5μM MG132 Treatment 69
Figure [14]: Flow Cytometry Analysis for Secondary Antibody Specificity 70

Chapter 1

Introduction

Introduction

1.1 Ataxia-Telangiectasia (AT):

AT is an ultra-rare, autosomal recessive disorder that results from mutations in the AT-mutated (ATM) gene (1-5). The disorder has an estimated incidence of around 1:100,000 live births, with a reported epidemiological range between 1:40,000 and 1:300,000 live births (1, 2, 4). It is mostly inherited in a complex heterozygous fashion, and depending on the mutation can manifest as a mild, classic or related syndrome (1, 4). The condition is so called because of its phenotypical hallmarks of ataxia, which results from neurodegeneration of Purkinje cells in the cerebellum, and telangiectasia, which manifests as prominent web-like blood vessels on the eyes and other mucous membranes (1, 2, 4). Cells from these patients are characterised by hypersensitivity to ionising irradiation, chromosomal instability and cell cycle abnormalities. Prognosis of is poor, with patients usually wheelchair-bound by teenage and passing away by their thirties (1, 4). Carriers of a mutated allele are at an increased risk of several of its complications, including cancer (1, 4).

Clinical manifestations of AT are multisystemic (1, 2, 4, 6). Ataxia may be accompanied with such neurological complications as extrapyramidal abnormalities, tremors and myoclonic jerks, all of which may interfere with voluntary movements (1, 4, 6). Dysphagia can lead to aspiration and nutritional deficiencies, whereas oculomotor complications can manifest as apraxia, nystagmus and strabismus (1, 4, 6). The leading cause of mortality is pulmonary deterioration, which manifests in more than 25% of patients as restrictive lung disease due to bronchiectasis, fibrosis and interstitial abnormalities (1, 4, 6). Primary immunodeficiency is common, and results from hypoglobulinaemia and lymphopenia (1, 4, 6). Complications include increased propensity for autoimmune, inflammatory and infectious diseases, with a particular prevalence of cutaneous granulomas (1, 4, 6). AT patients are also at significantly

increased risk of cancer, with up to 25% developing it throughout their lifetimes (1, 4, 6). Leukaemias and lymphomas are the most common in patients under twenty years of age, whereas various solid tumours are also common in adults (1, 4, 6). Endocrine and orthopaedic complications are variable, with the former including developmental disorders and insulin-resistant diabetes mellitus (1, 4, 6).

Current treatments are only supportive, and none interfere with disease progression (1, 4, 6). Neurological manifestations are mainly managed with occupational therapy, although anti-epileptic and anti-Parkinsonian drugs can be prescribed to manage involuntary movements (1, 4, 6). These include trihexyphenidyl, amantadine, pregabalin, baclofen, clonazepam, gabapentin and pregabalin (1, 4, 6). Immunodeficiency is managed with prophylactic antibiotics, immunoglobulin infusions and special vaccination schedules, whereas autoimmune and inflammatory complications are treated with corticosteroids, cyclosporine and tumour necrosis factor-α inhibitors (1, 4, 6). Pulmonary deterioration is managed with chest physiotherapy, breathe-aiding devices, bronchodilators, corticosteroids and antibiotics (macrolides, aminoglycosides and/or fluoroquinolones) (1, 4, 6). Cancer treatments for AT patients are different from those of the general population, as this group is sensitive to cyclophosphamide and ionising irradiation (1, 4). Ophthalmic and orthopaedic surgeries can also be indicated (4). AT management therefore requires multidisciplinary teams, frequent monitoring and personalised treatment regimens (1, 4, 6).

1.2 Molecular Biology of ATM:

ATM is a serine/threonine kinase that belongs to a protein family known as PI3K-like protein kinases (PIKKs), members of which have sequence homology to phosphatidylinositol 3-kinases (PI3K) (3-5, 7-9). ATM plays a crucial role in mediating the repair mechanism of DNA

double strand breaks (DSBs), by triggering the DNA damage response (DDR) (3-5, 7-9). It also coordinates cell cycle checkpoints, and orchestrates responses against oxidative stresses and various genotoxicities (3, 5, 7). Central to its function is the kinase domain, with which it phosphorylates downstream proteins in various signalling cascades (10, 11). As with other PIKKs, the kinase domain is respectively flanked at the N- and C-termini by domains known as FAT (FRAP-ATM-TRRAP) and FATC (FAT carboxy-terminal) (10, 11). The amino terminals of PIKKs consist of alpha-helical repeats, known as HEAT (Huntington-elongation factor 3 protein phosphatase 2A-TOR1) domains (10, 11). A schematic of the ATM sequence is shown in Figure [1]. ATM protein is large, compromising of 3,056 residues with a molecular weight of around 250kDa (10, 11). It exists in the inactive state as dimers or oligomers, and upon activation dissociates into functional monomers. It is mostly localised in the nucleus, but can associate with the cytoplasm, mitochondria and peroxisomes (4).

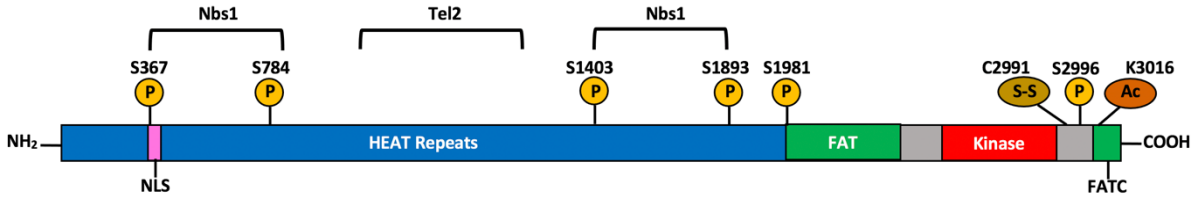


Figure [1]: Structure of ATM
This figure shows a schematic of the ATM sequence, highlighting key domains, post-translational modifications (PTMs), and interaction sites

Due to its size, the structure of ATM protein has not been resolved by X-ray crystallography (11). The structure of DNA-PKcs, a PIKK with which ATM has significant sequence homology, has been resolved by crystallography and electron microscopy (11). The overall structure is that of ring, with the kinase domain at the crown flanked by FAT and FATC (11). HEAT domains form the arm of the ring, and mediate interactions with DNA, regulatory agents and downstream proteins (11). They interact with the Tel2-Tti1-Tti2 (TTT) complex, which is

a PIKK-specific cochaperone that recruits heat shock protein-90 to ensure folding integrity (11). FAT and FATC regulate the effector kinase domain (10, 11). The former inhibits kinase activity in the inert state (10, 11). Upon activation ATM auto-phosphorylates serine residue S1981, which is located at the junction between FAT and HEAT repeats (10, 11). This induces a conformational change that liberates the kinase domain to interact with substrates (10, 11). FATC on the other hand harbours lysine residue K3016, which is acetylated by acetyltransferase Tip60 to augment ATM activation (11).

ATM is a master transducer of the DDR, and its recruitment is highly complex (10, 11). One induction pathway involves the Mre11-Rad50-Nbs1 nuclear complex (MRN), which directly binds DSBs (10, 11). It in turn interacts with the HEAT repeats of ATM by the N-terminal of Nbs1 (10, 11). Activation drives the accumulation of ATM molecules at the DSB site, as ATM phosphorylates the histone H2AX (11). Phosphorylated H2AX (γH2AX) binds the recruiter protein MDC1, which upon phosphorylation by ATM binds additional MRNs and ATM molecules (11). This oligomerisation process repeats such that the entire DSB region is flanked by ATM-MRN-MDC1 complexes (11). This activation process can be modulated by various regulatory agents, as explained below (11).

Once activated by DSBs, ATM initiates a complex yet structured signalling system (10, 11). Several ATM substrates are kinases themselves, thereby amplifying the ATM response by phosphorylating multitudes of downstream substrates (10, 11). Such kinases include CHK1, CHK2, MK2, HIPK2, DNA-PKcs and AKT (10, 11). Other substrates are cell fate regulators, such as p53, 53BP1, BRCA1, NF-KB and PIDD (10, 11). Yet others are direct effectors of DSB repair, such as Artemis, CtIP and RAD9 (10, 11). ATM activates several epigenetic factors, such as KAP1, RNF20-RNF40 and CHD4 (10, 11).

Due to its numerous roles and complex interactions, ATM expression is tightly regulated (10, 11). Several agents modulate MRN-mediated activation, such as apoptotic regulators AVEN and FOXO3A, histone acetyltransferase KAT8, effector recruiters 53BP1 and BRCA1, and ubiquitin ligases RNF8, SKP2 and CHFR (10, 11). ATM is subject to several regulatory posttranslational modifications (PTMs), which span residues beyond S1981 and K3016 (10, 11). PTM sites include phosphorylation residues S367, S784, S1403, S1893 and S2996, as well as the disulphide bridge residue C2991 (10, 11). Some of these PTMs are self-induced (10, 11). The nuclear localisation site controls nuclear ATM concentration (10, 11). Inactivation is driven by several phosphatases, including WIP1, PP2A and PP5 (10, 11).

In addition to its primary role in moderating DSB responses, ATM contributes to various other regulatory systems (8). It is a key agent in oxidative stress responses; it blocks the production of reactive oxygen species by mitochondrial oxidative phosphorylation, and stimulates the pentose phosphate cycle to increase the production of antioxidant NADPH (8). Redox stress due to ATM malfunction is thought to underlie Purkinje cell neurodegeneration in AT patients (4). ATM also modulates key components of the cell cycle, such as the mitotic spindle checkpoint system (4). This is thought to contribute to the immunological and oncologic complications of AT (4). ATM mediates cellular homeostatic responses to insulin, hypothermia, hypoxia and hypotonicity (10, 11). It however appears to only play a marginal role with single strand break (SSB) repair (10).

1.3 Experimental Therapies for AT:

Previous studies attempted to correct the AT phenotype in preclinical models by gene therapy. Early efforts aimed at the construction of stable plasmids carrying full-length ATM, and the demonstration of effective transfection *in vitro* (12, 13). Successful attempts made use of ATM

cloned into Epstein-Barr virus-based constructs, which could be transfected in human $ATM^{-/-}$ cells using $CaPO_4$ and Lipofectin™ (12, 13). These non-viral agents are however unsuitable for clinical use, due to their low *in vivo* transfection efficiencies and toxicities at high doses (14).

Viral vectors are more efficient in gene delivery than non-viral agents, with lentiviral (LV) and adeno-associated viral (AAV) vectors being the best clinically characterised (15). Payloads of viral vectors are however limited by capsid sizes (15). The 9.2kb ATM gene is well beyond the capacity of AAVs, which is limited at 5kb for genes delivered in the natural AAV conformation of single-stranded DNA (16, 17). AAV capacity is reduced to 2.5kb for the self-complementary double-stranded DNA conformation, which results in better transgene expression by bypassing the rate limiting step of second-strand synthesis (16, 17). ATM is at the threshold of the 9kb LV capacity, and functional LV titres are known to be compromised with such large inserts (16, 18). LVs are also associated with insertional mutagenesis, as they integrate randomly into host genomes (15). They however can be attractive vehicles for ATM delivery as they enable permanent genomic insertion, carry a low immunogenic risk, and transduce both dividing and non-dividing cells (15, 18). The last aspect is relevant to transducing post-mitotic Purkinje cells. A recent study examined ATM delivery *in vitro* using a third-generation LV, which employed the human elongation factor 1-α (hEF1A) promoter (18). These were tested for transduction of immortalised $ATM^{-/-}$ fibroblasts (18). The titre after purification was $5x10^6$ viral genomes/ml, which is low given that titres of the order 10^8 are needed for clinical use (18-22).

Herpes simplex type-1 amplicon vectors (HSVs) have been reported to efficiently shuttle ATM, owing to their large payload capacity of 150kb and efficient transduction of various mammalian cells (23-28). Early studies reported effective and functional transduction *in vitro* in $ATM^{-/-}$ cells (24), whereas later ones demonstrated *in vivo* delivery following intracerebral injection in

rats (27). Expression was comparable to endogenous levels, but did not persist beyond 13 days of administration (27). This implies that repeated administration may be needed for clinical efficacy, but this is precluded by HSV immunogenicity and by tissue injuries secondary to injection (27). To address this limitation, HSV/AAV hybrid vectors have been tested (26). These prolong ATM expression by integrating it into the AAVS1 site on human chromosome 19 (26). They however are associated with residual toxicity, have high pre-existing immunity in the general population, and may recombine with latent herpes simplex (15). Expression of AAV Rep protein may also decrease titres below clinically relevant levels (26, 29, 30).

An experimental therapy currently in Phase III trials is Erydex®, which comprises of low-dose dexamethasone delivered through autologous erythrocytes (31). Systemic corticosteroids partially alleviate AT symptoms, and intraerythrocytic delivery enables controlled release while limiting steroidal adverse effects (31). Phase II trials concluded that Erydex® can improve the neurological phenotype of AT and delay disease progression (31). Dexamethasone induces the expression of alternatively spliced ATM transcripts, such that exon skipping may bypass mutations upstream of the kinase domain (32-34). One well-characterised transcript is ATMdexa1, which encodes a truncated protein known as MiniATM that retains kinase activity *in vitro* (33, 34). This consists of the 251 C-terminal residues of ATM, which correspond to the kinase and FATC domains (33, 34). An alternative explanation is that dexamethasone induces the nuclear localisation of transcription factor NRF2, which stimulates expression of the antioxidants glutathione and NADPH (35, 36). These reduce the oxidative stress associated with high metabolic activity, thereby partially offsetting the loss of ATM function (35, 36). Given the complex function, interactions and regulation of ATM, this therapy is unlikely to completely compensate for the loss of the intact protein. Clinical trials for example do not report improvements in the immunological manifestations of AT (31).

Allogenic haematopoietic stem cell (HSC) transplantation is another experimental therapy for AT (37). The protocol involves depleting the bone marrow of HSCs by chemotherapy or irradiation conditioning, and engraftment of HSCs from HLA-matched donours (37). HSC transplantation in AT animal models alleviated immunodeficiency, reduced incidence of lymphomas, and improved longevity (38-40). HSC-derived cells repopulated the bone marrow, blood, thymus, spleen and lungs in $ATM^{-/-}$ mice, although they did not migrate to the cerebellum (39). Mortality rates of HSC transplantation in AT patients however remain unacceptable at around 75% within 35 months, most likely due to patient hypersensitivity to the conditioning regimens (37). Individual cases of AT patients who benefited from immunological reconstitution post-transplantation are however reported, both in pre-emptive and treatment clinical contexts (41, 42). Future advances such as reduced-intensity conditioning or targeted HSC antibodies may enable AT-specific allogenic transplantation regimens (41).

Genome editing, molecular mechanisms of which are explained in Section 1.6, is another experimental technique of relevance to AT treatment (43). One implementation aims at the development of CRISPR/Cas9 constructs for the targeted editing of specific ATM mutations, namely 5762ins137, 103C>T, 2T>C and 7638del9 (43). The first is an insertion mutation, wherein 137bp from intron 40 are transcribed at location 5762bp between exons 40 and 41 (43). This mutation results in accelerated ATM degradation, and accounts for 10-15% of AT cases in the UK (43). The second and third are missense mutations at locations 103bp and 2bp, whereas the last is a deletion of 9bp at the location 7638bp (43). This approach however does not provide a universal treatment for AT, thereby complicating the practical aspects of clinical and commercial translation (43). A different approach aims at employing CRISPR/Cas9 to insert either halves or the entirety of the ATM gene, with the target location being the AAV1 safe harbour site or the endogenous site (43). This requires inducing a DSB at the target location

by Cas9, followed by delivery of the ATM gene flanked by homologous ends (43). The study proposes the use of adenoviral vectors to deliver ATM, as these have the capacity to contain such large cargoes (43). Like HSVs, they are highly immunogenic and have high pre-existing immunity in the general population (15, 30, 43).

1.4 Experimental Methods for AT Therapeutics:

Several AT models exist for the *in vivo* development of experimental therapies. The classical model is a knockout mouse homozygous for the disrupted ATM gene, which displays such characteristic phenotypes as growth retardation, infertility, immunodeficiency and propensity to lymphoma (44, 45). Cells from this model replicate the hallmarks of hypersensitivity to γ-irradiation and oxidative stress, as well as of cell cycle abnormalities (44, 45). They do not replicate neurological manifestations of human AT (44, 45). One novel animal model consists of mice with tamoxifen-inducible wildtype ATM, which have been generated by bacterial artificial chromosome recombineering (46). This model demonstrates the feasibility of reversing the AT phenotype upon reconstitution of ATM expression, thereby highlighting the appropriates of gene therapy for this condition (46). A yet unpublished study reports a novel murine model that displays progressive ataxic neurodegeneration, thereby comprehensively replicating the human phenotype (47).

In vitro models consist of $ATM^{-/-}$ cells, usually characterised by heterozygous mutations that result in loss of ATM function. One commonly used primary $ATM^{-/-}$ cell line is GM07481 (Coriell Institute), which consists of fibroblasts derived from an AT patient with uncharacterised ATM mutations (24). One control against which it can be analysed is HFF-1 (ATCC® SCRC-1041™), a cell line of primary wildtype human fibroblasts. SV40-immortalised $ATM^{-/-}$ cell lines are also available, including GM9607 (Coriell Institute),

GM05849 (Coriell Institute; also known as AT5BIVA) and AT22IJE-T (Dr Shiloh's lab, Tel Aviv University) (27). Controls against which these can be analysed include the SV-40 immortalised cell lines GM0637 (Coriell Insitute), VA13 (ATCC), and GM16666 (Coriell Institute, also known as AT22IJE-PEBS7-YZ5 from Dr Shiloh's Lab, Tel Aviv University) (12, 27). The first is derived from healthy ATM-heterozygote human fibroblasts, and the second from normal human foetal lung fibroblasts (12, 27). The third consists of AT22IJE-T cells transfected with ATM cloned into pEBSt, which is an episomal replication-competent mammalian expression vector (12, 27, 48). Immortalised $ATM^{-/-}$ fibroblasts can also be generated from GM07481, by transduction with the human telomerase catalytic domain (18).

Immunostaining is a commonly used methodology to detect target proteins, and can be applied in three techniques to demonstrate expression of transfected ATM in various studies (18, 24-27). The first is immunocytochemistry, which involves permeabilisation of the cell membrane with such surfactants as Triton X-100 to facilitate antibody entry (24, 25, 27). Cells are stained with a primary antibody targeted to the translated protein, and with a fluorophore-conjugated secondary antibody that recognises the primary antibody (24, 25, 27). Fluorescence not only verifies transgene expression, but also localises the expressed protein within the cell (24, 25, 27). Mammalian cells can auto-fluoresce at wavelengths ranging between 350nm and 550nm, so fluorophores that either emit wavelengths outside this range or fluoresce very brightly can be chosen to reduce autofluorescence interference (49). Examples of fluorophores available in conjugation to secondary antibodies include Alexa Fluor®-647 and DyLight™-550, which have emission maxima respectively at wavelengths 668 nm and 550 nm (50, 51). Another immunostaining technique is Western blotting, wherein protein lysates are separated by gel electrophoresis and stained with primary and secondary antibodies (18, 24-27). The resulting band can be checked for the size of the target protein with a control ladder, so as to validate appropriate immunostaining (18, 24-27). The final technique is immunoprecipitation, wherein

the target protein-primary antibody complex is isolated from cellular lysates by protein A/G agarose beads (24-27). These bind antibodies, such that centrifugation separates the complexes from soluble proteins (24). This technique enables extraction of the expressed protein for direct analysis (24-27). Primary antibodies targeting ATM are available, but are of low specificity (24, 26). Several studies conjugate ATM with a flag tag, which consists of a flanking amino acid sequence that is detected by specific primary antibodies (24, 26).

The literature describes assays for examining functionality of transgenic ATM at the cellular level. These assess the viability of transfected $ATM^{-/-}$ cells following exposure to genotoxic stimuli, which would be lethal without adequate ATM function (18, 27). Sensitivity is assessed by colony forming assays, details of which are described in Section 5.2.1 (18, 52). These assess the ability of cells to form viable colonies after exposure to stress agents (18, 52). The most commonly used agent is ^{137}Cs γ-irradiation, sensitivity to which is a clinical hallmark of AT (18). Oxidative stress induced by t-butyl hydroperoxide has also been employed (27). ATM partakes in cellular responses to treatment with DSB-inducing cytotoxics, such as etoposide, topotecan and neocarzinostatin (53-59). Another assay examines cell cycle abnormalities post γ-irradiation (18, 24). $ATM^{-/-}$ cells undergo cell cycle arrest at the G2-M phase post-irradiation, such that the ratio $\frac{Number\ of\ Cells\ in\ G_2-M\ Phase}{Number\ of\ Cells\ in\ G_0-1\ Phase}$ can be used to assess the relative proportion of corrected cells (18, 24).

Molecular functionality assays detect the presence of direct ATM kinase substates in their phosphorylated states after exposure to ATM-activating stimuli (18, 24-27). Exemplar markers for ATM activation are phosphorylated p53 (p-p53) and γH2AX, for which primary antibodies exist (18). ATM also auto-phosphorylates its S1981 residue, and primary antibodies exist for such phosphorylated ATM (p-ATM) (18). Immunocytochemistry and Western blotting can be applied to examine the presence of these phosphorylated substrates after γ-irradiation of

transfected $ATM^{-/-}$ cells (18). An *in vitro* kinase assay is also described in the literature, wherein expressed ATM protein is immunoprecipitated and resuspended in a kinase buffer (24). This contains ATP radiolabelled with ^{32}P, as well as p53 as an ATM substrate (24). The substrate is analysed by Western blotting, and the corresponding band inspected for radiolabelling to confirm phosphorylation by ATM (24).

As ATM levels are tightly regulated, measures can be taken to enhance its detection in expression assays. One method to assess transgene expression involves fusing the target protein with a reporter protein, such as *Zoanthus* sp. green fluorescent protein (zsGreen) (60). This protein has excitation and emission maxima respectively at wavelengths 496 nm and 506 nm (60-62). Fusion via self-cleaving peptides can couple expression of ATM and zsGreen, while rescuing the latter from co-degradation with the former (63, 64). This in turn may enhance fluorescence detection by microscopy and flow cytometry. A schematic of T2A decoupling is shown in Figure [2]. Cells can also be treated with agents that stabilise ATM intracellular concentrations, such as the histone deacetylase inhibitor known as vorinostat or suberanilohydroxamic acid (SAHA) (65). This reagent epigenetically enhances expression of endogenous genes by promoting the accumulation of acetylated histones, which prolongs interactions of transcription factors with promoters (65). Its mechanism with episomal constructs may be different, and evidence exists that it specifically interacts with DDR systems by inducing DSBs and modifying chromatin (66). Its effect on ATM expression appears to be cell-line specific(67). It was found to promote accumulation of activated ATM proteins in cancerous cell lines, but to mitigate ATM expression in transformed cell lines (67). MG132 is a proteasome inhibitor that interferes with the degradation of ubiquitinated proteins, and thus can increase intracellular half-life of ATM (68). Finally, ATM expression can be stimulated by treatment with DSB-inducing stimuli as for functionality assays (8, 9, 18, 24-27, 69-72).

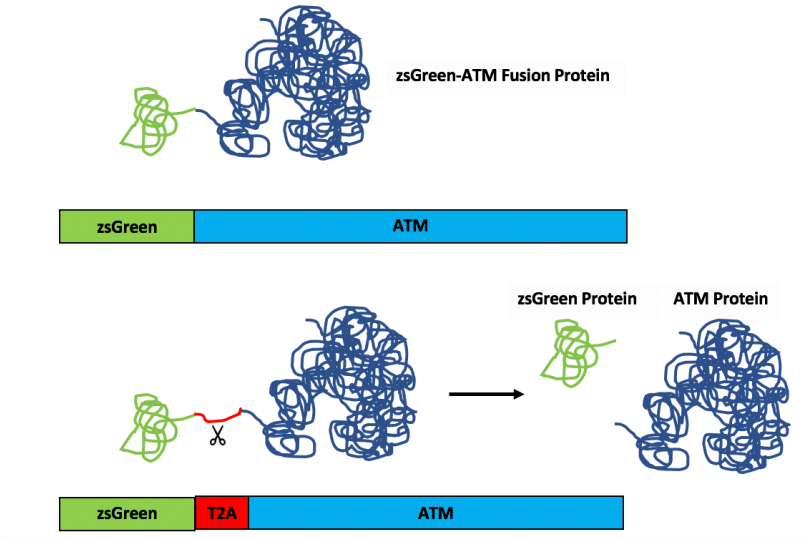


Figure [2]: Protein Fusion via Self-Cleaving Peptides
This schematic highlights how T2A self-cleavage ensures co-expression of reporter and ATM proteins, while preserving the former from co-degradation with the latter

Other experimental tools are described in the literature that could aid in the development of AT gene therapies. Evidence for genomic integration of ATM can be obtained where relevant by PCR of isolated genomic DNA, using primers specific to the transfected sequence (18, 26). Non-immunostaining expression assays include reverse transcription PCR (RT-PCR), wherein messenger RNA (mRNA) sequences specific to the ATM transcript are reverse-transcribed to DNA and amplified by PCR to confirm transcription (18, 25). Nuclear localisation after irradiation can be validated by extracting the nuclear lysate using commercial nuclear extraction kits, and Western-blotting the samples for ATM and/or p-ATM (18). The construct pLV.ATMi (Addgene #14542) encodes short hairpin RNA (shRNA) that knockouts ATM expression, and can be used to study loss of ATM function in cells of wildtype genotype (73).

1.5 Glycosaminoglycan-Enhanced Transduction:

Glycosaminoglycan-enhanced transduction (GET) is a non-viral delivery technique, that is based on fusion peptides that couple cell-penetrating peptides (CPPs) with membrane-docking

peptides (MDPs) (74-76). CPPs are transduction domains that enable intracellular delivery of conjugated macromolecules by inducing endocytosis (74). Their conjugation versatility and transduction efficiency could make them ideal delivery vectors, but they suffer from low cellular targeting efficiency (74). Fusion with MDPs synergistically overcomes this limitation, as these interact with proteoglycans expressed on cell membranes (74). MDPs do not induce cellular uptake themselves, but their fusion enhances CPP-mediated endocytosis by up to two orders of magnitude (74). Currently the best characterised MDPs target the glycosaminoglycan heparan sulphate, which is expressed ubiquitously on animal cells (74). GET peptides have been proven to mediate efficient delivery of functional enzymes, antibodies, nucleic acids, transcription factors, and magnetic nanoparticles in various cell types (74-77).

GET peptides provide a promising platform for gene delivery. Owing to their positive charges, they form direct electrostatic interactions with the negatively charged phosphate groups of unconjugated plasmid DNA (pDNA) (74-76). This interaction can result in stable transfection nanoparticles (74). Such complexation has been demonstrated by a fluorescence-based assay, using the dye YO-PRO1 that fluoresces upon DNA binding and competes with GET peptides for pDNA complexation (75). Increasing the charge ratio of peptide positive charge : pDNA negative charge enhances complexation, with out-competition of YO-PRO1 resulting in decreased fluorescence (75). Higher charge ratios may also increase nanoparticle stability, as they result in increased ζ-potentials and decreased hydrodynamic sizes (75). GET peptides can be formulated in a variety of manners to optimise gene delivery. GET nanoparticles for instance can be PEGylated, which could result in charge shielding, increased half-life and enhanced biodistribution (74-76). Alternatively, the peptides can be formulated to deliver poly (lactic-co-glycolic acid) (PLGA) microparticles encapsulating the constructs of interest, thereby protecting pDNA from nuclease-mediated degradation (74-76). Peptides can be designed to

incorporate MDPs that interact with proteoglycans that are differentially expressed on certain cell types, thereby enabling specific targeting (74-76).

GET peptides can be modified to control their pDNA transfection properties (74). One of the earliest GET peptides to demonstrate pan-nucleic acid transfection with efficiency comparable to Lipofectamine® is PLR, which has the sequence P21-LK15-8R (74). P21 acts as the MDP, is the heparin-binding domain of the heparin-binding epidermal growth factor, and has the amino acid sequence (KRKKKGKGLGKKRDPCLRKYK)(74). LK15 is an amphiphilic peptide that interacts with nucleic acids, and has the sequence (KLLKLLLKLLLKLLK) (74). 8R is a positively-charged CPP that mediates efficient endocytosis, and is composed of eight arginine residues (74). Further nucleic acid-binding GET peptides have been developed based on this design, by changing the MDP and/or CPP (74-76). These include FLR (FGF2B-LK15-8R) and FLH (FGF2B-LK15-10H) (74-76). Both have FGF2B as the MDP, which is the heparin sulphate-binding domain of the fibroblast growth factor 2, and LK15 as the nucleic acid interacting region (74-76). FLR has 8R as the CPP, and so is suited to induce endocytosis (74-76). The delivery it mediates however results in poor expression due to endosomal trapping (74-76). FLH has 10H as the CPP, which is composed of ten histidine residues. This peptide mediates poorer cell penetration than FLR, but superior endosomal escape (74-76). This is because imidazole side chains of poly-histidine sequences have a pKa of 6.0, which is below the pH of mature endosomes (78). Protonated histidines directly disrupt endosomal membranes, and act as “proton sponges” that induce endosomal swelling by increasing osmolarity (78). Incorporation of FLR and FLH has synergistic delivery effects, as they respectively mediate efficient endocytic uptake and endosomal escape (74-76). Schematics of the structures of FLR and FLH, and of their interactions with pDNA to form transfection nanoparticles, are shown in Figure [3] below.

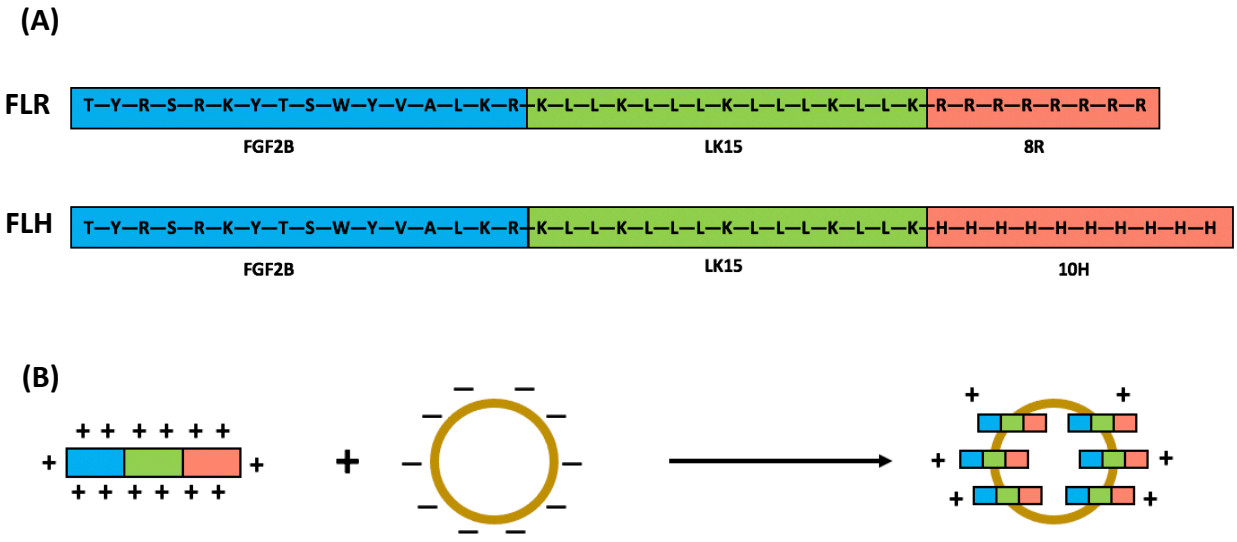


Figure [3]: Structures of GET Peptides and Nanoparticles
(A) These schematics capture the structures of GET peptides FLR and FLH. Blue designates the MDP, green the amphiphilic sequence, and red the CPP. (B) This schematic captures the complexation of GET peptides with pDNA to form positively charged transfection nanoparticles

GET vehicles offer several advantages over alternative gene delivery techniques. Their biosafety profile is superior to that of viral vectors, as, GET nanoparticles pose minimal risks of immunogenicity, insertional mutagenesis, and recombination with latent infections (74, 75). Other advantages include simplicity and cheapness of manufacture (74, 75). LV and AAV transductions are significantly more efficient than GET for the delivery of constructs within their payload capacities (15, 74). GET however is not restricted by capsid size, and may be more suitable for the efficient transfer of large constructs. GET peptides mediate greater transfection efficiencies than several other non-viral vectors (74, 75). The FLR/FLH synergy bypasses the need for excessively high CPP charges to mediate efficient transfection, which is advantageous as these can be toxic (74, 75).

GET delivery is associated with several limitations that need to be addressed in formulation development. These include reliance on endocytic uptake, which naturally is more efficient for

smaller cargoes (74). This aspect can be addressed by optimising the relative content of GET peptides to pDNA (75, 79). Endosomal escape is a major obstacle, and may require optimisation of the relative amounts of FLR and FLH to arrive at the best compromise between cellular uptake and endosomal escape. Nanoparticles also need to be designed for *in vivo* performance, which encompasses optimisation of such pharmacokinetic and biopharmaceutics properties as release, distribution and elimination (75). Pharmacodynamic development seeks to optimise transfection and expression in the target organ, which may be hindered by drug delivery barriers(75). Such developments may require the incorporation of excipients, the relative amounts of which may require optimisation (75, 76). GET-delivered pDNA also needs to localise in the nucleus for expression, which may require such modifications as the incorporation of nuclear localisation sequences in plasmids (75).

1.6 Implementation of GET Gene Therapy:

GET-mediated gene therapy can be implemented through various modalities, three of which are described in the literature. The first is based on uptake of nanoparticles resulting directly from the complexation of GET peptides and pDNA (75), and has been examined for the pulmonary delivery of pDNA encoding luciferase (75). Pulmonary delivery is challenging to viral and non-viral vectors alike, as the mucus barrier impedes vector diffusion and transfection (80, 81). The optimal GET formulation consisted of pDNA complexed with 40% PEGylated FLR, which presented a transfection profile superior to those of polyethylenimine and Lipofectamine® in biosafety and/or efficiency (75). PEGylation in this study highlights the versatility of GET peptides, which can be modified as per transfection requirements (75). Although it reduced transfection efficiency *in vitro* by impeding GET peptides from interacting

with cell membranes, controlled PEGylation overall enhanced transfection *in vivo* by improving nanoparticle stability and distribution in mucus (75).

The second modality involves encapsulating pDNA with biodegradable polymers, followed by complexing these polymers with GET peptides (82). This technique was applied in osteogenic tissue engineering, wherein plasmids encoding transcription factor BMP2 were encapsulated in PLGA microparticles (82). Complexation with GET peptides enhanced intracellular uptake of these microparticles by up to sevenfold, and transfection efficiency by up to five orders of magnitude (82). The design protected pDNA from nuclease-mediated degradation, and induced osteogenic development in mesenchymal stromal cells (82). Such formulations can be modified to optimise transfection (82). PLGA is FDA-approved for human use owing to its favourable biosafety profile (82). Acidic byproducts of its biodegradation however interact unfavourably with GET peptides, thereby interfering with transfection efficiency (76). Optimal formulations co-encapsulate the pH-activated excipient L-histidine, which when exposed to the acidic environment of biodegradation complexes with PLGA byproducts (76).

The final modality is based on the delivery of GET-conjugated recombinant proteins that modulate gene expression (83). It differs from the previous two in that it does not involve direct pDNA delivery, but instead relies on the uptake of transcription or growth factors to induce lineage-specific gene expression (83). The modality is particularly suitable for tissue engineering (83). Proteins are tagged on the N-terminus with the MDP domain, and on the C-terminus with the CPP domain (83). One study demonstrated delivery of GET-tagged myogenic differentiation master regulator (MyoD) using a gelatine-agarose hydrogel, and confirmed the induction of myogenic gene expression in HEK293T cells (84). Another established the delivery of GET-tagged Runt-related transcription factor 2 (RUNX2), and confirmed induction of osteogenic gene expression in mesenchymal stem cells (83). Formulations can be modified for optimal protein delivery. One study for example described

encapsulation of GET-conjugated RUNX2 in porous PLGA microparticles, and demonstrated the controlled release, uptake and functionality of the transcription factor (85). These microparticles were incorporated into a 3D-printable PLGA/PEG scaffold, and were verified to induce osteogenic gene expression and differentiation in loaded stem cells (85).

The first two modalities of GET-mediated gene therapy depend on the delivery of plasmids engineered for mammalian expression. One relevant construct is pGM169, which is a circular plasmid that has been clinically trialled for the gene therapy of cystic fibrosis (80). A schematic of this plasmid is shown in Figure [4]. It has been designed to be CpG-free, as CpG dinucleotides may be inactivated by methylation in mammalian cells (80, 86). They can also induce adverse inflammatory effects in humans, so their removal renders plasmids safer for repeat dosing (80). The transgene in pGM169 is cystic fibrosis transmembrane conductance regulator (CFTR) gene (80). It is under the control of the hCEFI promoter, which is composed of the hEF1A promoter combined with the cytomegalovirus (CMV) enhancer sequence (80, 86). This has been demosntrated to promote sustianle expression of the transgene up to two months (80, 86). Polyadenylation is needed in eukaryotic cells for the translation of mature mRNA, so the bovine growth hormone polyadenylation (BGH polyA) sequence is included immediately after the transgene (80). The plasmid contains the R6K bacterial origin of replication, and the kanamycin resistance gene under the control of bacterial promoter EM7 (80). Plasmid pGM169 is also known as pG4-hCEFI-soCFTR2 (86). The first component of this nomenclature indicates it is a fourth-generation CpG-free plasmid, which comprises a family of plasmids with the aforementioned backbone structure (the indicated origin of replication, polyA sequence, and antibiotic resistance gene) (86). The second and third components respectively indicate the promoter and transgene (86). The pG4 family was developed from an initial pG1 series, the CpG content of which was sequentially depleted and

backbone structure optimised to result in pG2, pG3 and pG4 plasmids (86). Family pG4 is compliant with pDNA requirements for investigational pharmaceuticals (86).

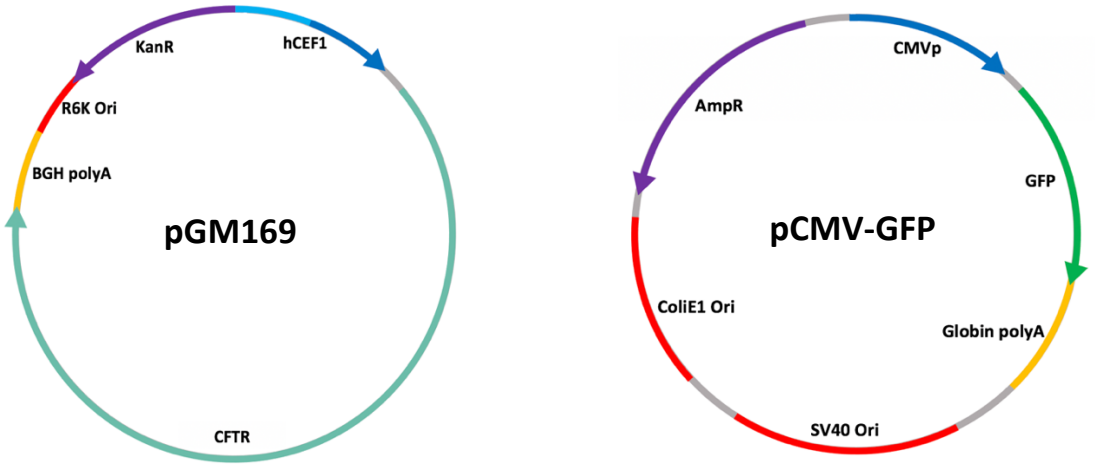


Figure [4]: Structures of pGM169 and pCMV-GFP
These schematics capture the structures of the pGM169 and pCMV-GFP plasmids. Blue designates promoter, green the transgene, yellow the polyA, red origins of replication, and purple antibiotic resistance gene

Construct pCMV is another plasmid designed for mammalian expression of transgenes (87). A schematic of this plasmid is shown in Figure [4]. Unlike pGM169, it is not CpG-free (87). The constrcut is under the control of CMV enhancer and promoter sequences (CMVp) (87). This mediates higher initial expression than hEF1A or hCEFI, but its expression profile is less sustainable (80, 86). The polyadenylation sequence used is that of beta-globin (87). For selection of transformed bacteria, the plasmid includes the ampicillin resistance gene (AmpR) under the control of the AmpR promoter (87).

One modality not yet explored for GET gene therapy involves its combination with genomic integration. Episomal pDNA is subject to inactivation by degradation, nuclear delocalisation or methylation (86, 88). Codon optimisation, removal of CpG sequences and incorporation of nuclear localisation signals may only prolong transient expression (86, 88). Episomal bacterial

plasmids do not replicate in the mammalian cell cycle, and so the transfected population of mitotic cells undergoes continuous dilution without repeat administration (80, 86, 88). Genomic integration enables permanent transgene augmentation (89). Transposases such as sleeping beauty can mediate the integration of large constructs, but their integration profiles are unstable, transient and random (90, 91). They are therefore subject to insertional mutagenesis (90, 91). Site-directed gene editing bypasses this risk, and is mediated by zinc-finger nucleases, transcription-activator like effector nucleases, and CRISPR-associated protein 9 (Cas9) (89). Wildtype Cas-9 is readily programmable as it is site-directed by guide RNA (gRNA) strands, such that it induces DSBs at the desired locations (89). Transfected genes can then be integrated at the DSB site by cellular machinery in a mechanism known as homology-directed repair (HDR), given that the gene is flanked by ends that are homologous to those of the DSB (89). HDR is inefficient for large inserts, thereby favouring alternative error-prone repair pathways(89). Non-homologous end joining (NHEJ) is such a mechanism, wherein the DSB ends are ligated directly by non-homologous indels (89). Another shortcoming of wildtype Cas9 is that the cell needs to go through the S-phase in mitosis for HDR to occur, and so is unsuitable for post-mitotic cells (89). Fusion proteins coupling catalytically-inactivated site-directing domains with functional transposase domains, such as the dCas9-Hsmar1 fusion protein, could enable the targeted integration of large genes in post-mitotic cells (92, 93). Such fusion proteins could be GET delivered as pDNA or recombinant proteins (74, 94). The latter however is preferred, as the former may result in toxic overexpression of the DSB-inducing agent and off-target mutations (94).

1.7 Implementation of GET for ATM Delivery:

Previous unpublished work from the Dixon Lab at the University of Nottingham has investigated the non-viral delivery of ATM pDNA by GET (95). The relevant results from these unpublished studies are summarised here to provide context for this project, which was a follow-on study. Initially, Branter et al characterised the physicochemical properties of these GET nanoparticles, which consist of FLR and FLH directly complexed with pDNA. Formulations containing constructs of various sizes were analysed by dynamic light scattering and laser Doppler anemometry. In order of increasing size, the constructs carried zsGreen, zsGreen-miniATM fusion and zsGreen-ATM fusion transgenes. Direct positive correlation was found between plasmid size and ζ-potential, suggesting that larger plasmids form more stable nanoparticles. Plasmid size was found to correalte positively with nanoparticle mobility, and negatively with each of conductivity and Z-diameter. This suggests that larger plasmids form nanoparticles with smaller hydrodynamic diameters. Nanoparticles of the largest construct had the lowest size polydispersity, suggesting they are the most homogenous. One explanation for these trends is that larger plasmids form a greater number of interactions per pDNA molecule with GET peptides, resulting in stronger overall interaction per plasmid. Another explanation is that size limits the stoichiometric conformations amenable to complexation. Both cases would result in more compact, stable, and uniform complexes for larger constructs. Nanoparticle sizes ranged between 110nm and 140nm, and ζ-potentials between 30mV and 35mV. Nanoparticles smaller than 150nm are subject to endocytic uptake (96), and ζ-potentials greater than 25mV indicate good pharmaceutical stability (97). The nanoparticles in this study are thus compliant with the properties required for efficient transfection.

Transfection of HeLa cells with these nanoparticles was also demonstrated by Branter et al (95). Transfection efficiency was assessed by examining the percentage of cells displaying

zsGreen fluorescence, using confocal microscopy. Positive correlation was found between transfection efficiency and pDNA dose for zsGreen protein and zsGreen-miniATM fusion constructs. Such dose dependency precludes the existence of a saturable cellular uptake method at the pDNA doses tested, which may otherwise impose an upper threshold on maximal transfection efficiency. Transfection efficiency was higher with the former construct, as were the efficiency enhancements of its uptake with pDNA dose escalation. Transfection efficiency may therefore negatively correlate with plasmid size, despite the larger constructs forming smaller nanoparticles that may be more amenable to endocytosis. This may be explained in terms of the plasmid size interfering with endosomal escape and/or transgene expression. Fluorescence was not observed with the zsGreen-ATM fusion construct. One explanation is that its large size significantly interferes with transfection efficiency, endosomal escape and/or transgene expression. Another is that ATM expression is tightly regulated, such that its short half-life limits visualisation of the fusion protein. The ATM protein may also be directly interacting with coupled zsGreen, in a manner that interferes with the latter's fluorescence.

Branter et al then optimised experimental conditions for the expression of transfected ATM in HeLa cells, as assessed by flow cytometry for fluorescence of covalently fused zsGreen (95). It was first found that the use of complete transfection medium results in greater expression, as compared to the use of serum-free medium. Transfection efficiencies of around 10% were later achieved, by treating transfected cells with SAHA. These results confirm that transfected plasmids may not express ATM efficiently without such stabilisation regimens, leading to underestimation of GET transfection efficiencies. Although SAHA and MG132 boost intracellular ATM protein concentrations by different mechanisms, co-treatment was not found to result in a synergistic stabilising effect. Finally, transfection efficiencies were compared in 3T3 and HeLa cells. The former may better model target $ATM^{-/-}$ cells as both are diploid, whereas HeLa cells are hyper-triploid. Higher expression levels of ATM however were

consistently achieved with HeLa cells, so these were deemed more suitable for assessing transfection improvements in optimisation experiments than 3T3 cells.

Experiments by Branter et al also demonstrated transfection of ATM pDNA in $ATM^{-/-}$ cells (95). Such investigation is necessary, as $ATM^{-/-}$ cells are ultimately the target cells for AT gene therapy. FLR and FLH are not cell-specific, as their MDPs target heparan sulphate that is ubiquitously expressed by mammalian cells (74). Factors improving transfection efficiency in one cell line may therefore apply to others. As seen with 3T3 and HeLa cells however, inherent cell line variations such as mitotic and chromosomal properties may interfere with result translatability. $ATM^{-/-}$ cells were transfected in complete medium, treated with SAHA, and analysed by flow cytometry for fluorescence of zsGreen fused to ATM. Transfection efficiencies between 5% and 10% were achieved, and these were deemed to correspond to those observed with HeLa cells.

Branter et al then enhanced the observed transfection efficiency by structurally decoupling zsGreen from the ATM protein post-expression (95). ATM protein may interact unfavourably with the fluorescence of fused zsGreen, and its instability may induce co-degradation of covalently linked zsGreen. Decoupling zsGreen may thus enhance fluorescence integrity, rendering the correlation between measured fluorescence and actual transfection efficiency more robust. Constructs fusing zsGreen to ATM or MiniATM via T2A were therefore transfected in $ATM^{-/-}$ and HeLa cells, and analysed by flow cytometry for zsGreen fluorescence. T2A linkage significantly enhanced the observed transfection efficiency of MiniATM constructs in both cell lines. This finding highlights that permanent fusion of zsGreen can indeed compromise fluorescence integrity, thereby underestimating true transfection efficiency. Nevertheless, T2A linkage did not significantly enhance the observed transfection efficiency of ATM constructs in either cell line. This can be explained in terms of the larger plasmids having less efficient endosomal escape and/or transgene expression. ATM

is a large protein that may not only interfere with zsGreen fluorescence, but also with T2A self-cleavage. ATM also has more regulatory domains than MiniATM, which may be subject to additional PTMs that accelerate degradation before decoupling.

Immunostaining was attempted by Branter et al to validate expression of transfected ATM (95). As primary antibodies against ATM protein are of low specificity, ATM was conjugated to a flag-tag for which specific primary antibodies are commercially available. The secondary antibody was conjugated to the fluorophore DyLight^{TM}-550, which has a wavelength distinct from that of zsGreen fluorescence. This enables effective resolution of the two signals in analysis. Transfected cells were treated with SAHA and the nuclear stain DAPI, and analysed by confocal microscopy. Constructs tested encoded untagged negative controls, ATM tagged with one flag sequence under the control of hCEF1 and CMVp promoters, and ATM tagged with two flag sequences under the control of hCEF1 promoter. Negative controls stained negative, thereby confirming lack of nonspecific binding of the secondary antibody. All flag-tagged constructs stained positive, although the signals generated were faint. This faintness precluded establishing the effects of promoter choice and tag number on ATM visualisation.

Rescue assays were designed by Branter et al to establish functionality of transfected ATM, in terms of reconstituting resilience of ATM$^{-/-}$ cells to cytotoxic treatment (95). Dose-viability experiments were first conducted, to determine baseline IC_{50} values of various cell lines to DSB-inducing agents. Cytotoxics tested were chloroquine, topotecan, neocarzinostatin and etoposide. Cell lines tested were ATM$^{-/-}$ fibroblasts, U87, KNS-42, HeLa, 3T3 and Hu-ES7-F1B. Transfected and control cells of each line were then treated with their respective IC_{50} doses of cytotoxics, and the percentage of viable cells was calculated using the PrestoBlue assay and UV-vis spectroscopy (98). Various constructs, cytotoxic regimens, and transfection conditions were examined. ATM transfection did not enhance viability post-treatment compared to controls in any cell type. This could either indicate that the transfection efficiency

of ATM is too low to offset the endogenous loss of function, or that cytotoxic assays are suboptimal for assessing ATM functionality. ATM is better characterised for its role in DSB repair post irradiation and oxidative stress, which may be more suitable challenge agents for such rescue assays.

The aforementioned results prompted Branter et al to investigate whether cytotoxic treatment is a suitable assay to demonstrate functionality of transfected ATM (95). The cells tested were HeLa and $ATM^{-/-}$ cells treated with pLV.ATMi, and either left untransfected or transfected with one of various ATM-encoding constructs. Negative controls were untreated with topotecan, whereas test cells were treated with their relevant IC_{50} doses of topotecan. Compared to their respective negative controls, viabilities of topotecan-treated cells tested uniformly fell to 50%. This was regardless of pLV.ATMi treatment or ATM transfection. This suggests that modulating ATM levels in HeLa cells does not significantly affect resilience to topotecan treatment. One reason behind this could be that ATM is not as central to mediating topotecan-induced DSBs, as it is to those induced by irradiation or oxidative stresses. Future functionality assays would therefore need to incorporate appropriate challenge agents.

1.8 Aims & Objectives:

The Dixon Lab at the University of Nottingham is running a proof-of-concept project for the feasibility of employing GET for AT gene therapy. This MRes study is part of the preclinical phase, and aims to optimise the GET formulation for efficient *in vitro* transfection of ATM pDNA. Experiments employed HeLa cells, owing to their ease of culture and amenability to transfection. This renders them ideal for formulation optimisation, prior to testing in $ATM^{-/-}$ cells. The following three objectives were set to achieve this study's aim:

- Optimising the relative amounts of GET peptides and pDNA in the formulation

- Optimising the treatment regimen for stabilisation of ATM expression
- Establishing expression of transfected ATM by immunostaining

The first objective seeks to optimise the relative contents of pDNA and peptides in the formulation, by establishing whether increasing the peptide : PDNA mass ratio (PDMR) enhances transfection efficiency of ATM in HeLa cells. The main goals of this objective are:

- Characterising the transfection profile of each GET peptide when employed alone at an elevated PDMR
- Determining the transfection efficiency of using FLR and FLH in combination at elevated PDMRs
- Establishing whether synergy between FLH and FLR persists at elevated PDMRs
- Establishing whether FLH-FLR synergy or PDMR elevation better contributes to the observed transfection efficiency
- Establishing the extent to which the size of ATM constructs interferes with the relationship between PDMR and transfection efficiency

The second objective seeks to optimise the treatment regimen for stabilising ATM expression, by establishing whether proteasomal inhibition can stabilise expression of transfected ATM in HeLa cells. The main goals of this objective are:

- Establishing whether proteasomal inhibition with small molecules can enhance expression of transfected ATM
- Determining whether histone deacetylase or proteasomal inhibition results in a greater stabilisation effect on ATM expression

- Establishing whether co-treatment with histone deacetylase and proteasomal inhibitors results in a synergistic effect on ATM stabilisation

The final objective seeks to establish ATM expression by immunostaining. The motivation is to demonstrate the presence of translated ATM proteins, by directly binding them with targeted antibodies. The main goal of this objective is:

- Validating translation of transfected ATM by immunostaining, as analysed by flow cytometry and confocal microscopy

Chapter 2

Materials & Methods

Materials & Methods

2.1 Materials:

2.1.1 Plasmids:

Plasmids were designed and synthesised *de novo* by Genewiz and Eurofins MWG, transformed into *E. coli*, and purified by the Qiagen® maxiprep kit. Concentrations were measured with Nanodrop™ microvolume spectrophotometer (ThermoFisher Scientific). The core plasmids into which the transgenes were cloned were pG4-hCEFI (pGM) and pCMV, backbone structures of which are shown in Figure [5] (86, 87). Descriptions of these plasmids are provided in Section 1.6. The nomenclature used for plasmids and transgenes in this study is presented in Table [1]. Figure [6] shows schematics of all the transgenes employed in the various constructs of this study.

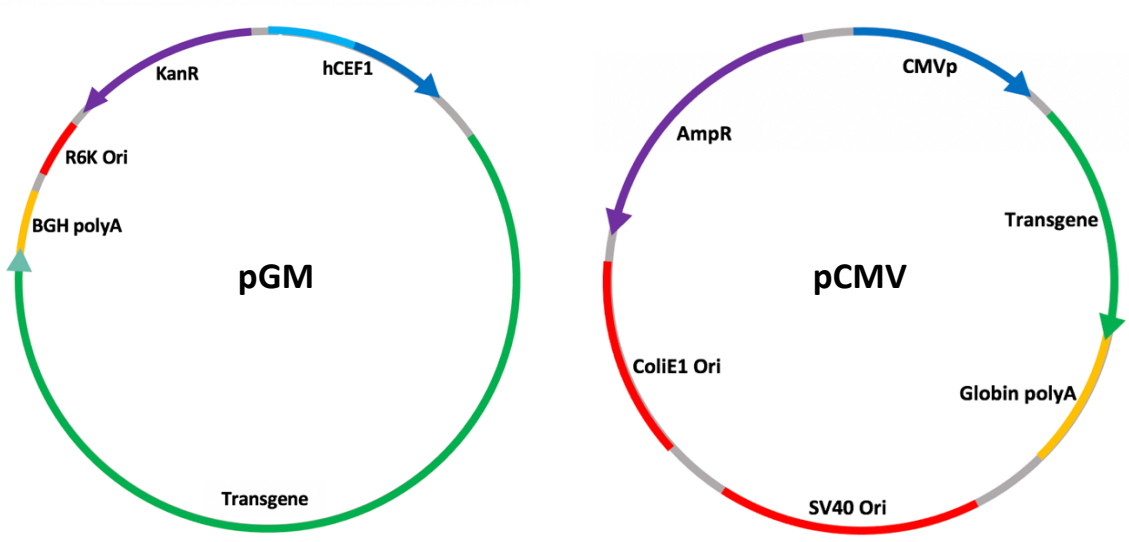


Figure [5]: Backbone Structures of Plasmids pGM and pCMV
These schematics show the backbone structures of plasmids pGM and pCMV. The transgenes employed in this study correspond to those shown in Figure [6]. Green denotes the transgene, blue the promoters, yellow the polyA sequences, red the origins of replication, and purple the antibiotic resistance genes.

Term	Explanation
pGM	Plasmid pG4-hCEFI, which is engineered to express transgenes under the control of CMV enhancer/hEF1A promoter in mammalian cells (86)
pCMV	Plasmid pCMV, which is engineered to express transgenes under the control of CMV enhancer/CMV promoter in mammalian cells (87)
zsGreen	Gene for *Zoanthus* sp. green fluorescent protein, used as an expression reporter (60-62).
ATM	Full-length, intact ATM gene
MiniATM	Truncated ATM gene, which corresponds to the spliced variant of ATM expressed after EryDex® induction (33)
T2A	Self-cleaving T2A peptide (Sequence: GSGEGRGSLLTCGDVEENPGP), used to decouple the zsGreen protein from the ATM and MiniATM proteins post-expression (64)
F	Flag tag (amino acid sequence: DYKDDDDK) targeted by the primary antibody (99)
H	Poly-histidine tag
Glux	Gene for *G. princeps* luciferase, used as a reporter bioluminescent protein (100)

Table [1]: Nomenclature of Transfection Constructs
This table explains the nomenclature used to describe plasmids and transgenes in this study

2.1.2 Cell Lines:

HeLa cells were obtained from ThermoFisher Scientific. Primary $ATM^{-/-}$ fibroblasts were obtained from Professor Malcolm Taylor of the University of Birmingham, and immortalised $ATM^{-/-}$ fibroblasts from Professor Ignacio J Molina of the University of Granada.

2.1.3 Reagents:

The GET peptides used were FLR and FLH, which were synthesised by SynPeptide. Sequences and structures of these are explained under Section 1.5. The primary antibody used for immunostaining was MA1-91878 (Invitrogen), which is a mouse antibody targeting the flag (DYKDDDDK) tag (99). The secondary antibody used was ab150115 (Abcam), which is a goat anti-mouse antibody conjugated with the Alexa Fluor®-647 fluorophore (50). OptiMEM®, Dulbecco's Modified Eagle Medium (DMEM), foetal calf serum (FCS), penicillin-streptomycin (P/S), antibiotic-antimycotic (AB/AM) and l-glutamine were obtained from Gibco, Thermo Fisher. Hoescht® stain was obtained from Invitrogen. 100% Methanol (MEth), 4% paraformaldehyde (PFA), Triton X-100, β-mercaptoethanol, SAHA, Tween® and MG132 were obtained from Sigma-Aldrich.

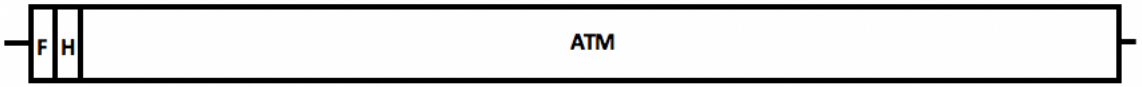
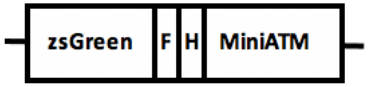
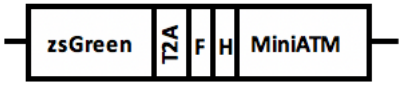
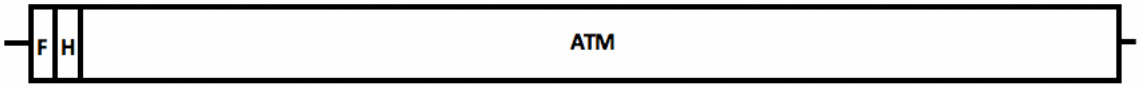
Construct	Plasmid	Transgene
pGM-Glux	pGM	
pGM-zsGreen	pGM	
pGM-F-H-ATM	pGM	
pGM -F-H-MiniATM	pGM	
pGM-zsGreen-F-H-ATM	pGM	
pGM-zsGreen-F-H-MiniATM	pGM	
pGM-zsGreen-T2A-F-H-ATM	pGM	
pGM-zsGreen-T2A-F-H-MiniATM	pGM	
pCMV-F-H-ATM	pCMV	

Figure [6]: Structures of Transgenes Employed in this Study
This figure shows schematics of the various transgenes employed in this study

2.2 Methods:

2.2.1 Cell Culture:

The growth medium used for HeLa cells was DMEM supplemented with 10% FCS, 100U/mL P/S, 100U/mL AB/AM and 2mM l-glutamine. The growth medium for $ATM^{-/-}$ cells was DMEM supplemented with 20% FCS, 100U/mL P/S, 100U/mL AB/AM, 2mM l-glutamine and 0.05mM β-mercaptoethanol. Before splitting cells, growth medium was removed from the T175 flask and cells were washed with phosphate-buffered saline (PBS). Then 3mL 0.1% trypsin-EDTA was added to each flask, and HeLa cells were incubated at 37°C for 3 minutes until they detached. Other cell lines required incubation up to 10 minutes. Trypsin was neutralised with growth medium in a ratio of at least 1:1. The average number of cells was counted by adding 10μL cell suspension into the haemocytometer, and concentration was calculated in terms of number of cells per mL.

2.2.2 Transfection:

A total of 40,000 cells were seeded per well on 20mm coverslips in 12-well plates for microscopy, whereas 100,000 cells were seeded per well in 12-well plates for flow cytometry. Each well was filled up to 1mL with growth medium and cells were incubated for 24h, to ensure a confluency of around 70% on day of transfection. Aliquots of the plasmid and 1mM peptide reagents were thawed out, allowed to reach room temperature and gently mixed by pipetting. OptiMEM was pre-warmed to room temperature. To a sterile microfuge tube, OptiMEM was added so that the final volume after adding the DNA was 50μL; 1.00μg pDNA was then added and the solution mixed. To a separate sterile microfuge tube, OptiMEM was added so that the final volume after adding the peptides was 50μL. Among the formulations examined in Sections 3.1 for transfecting 100,000 cells, the optimal one was found to incorporate both

16.32µg FLH and 15.22µg FLR for each 1.00µg pDNA. The peptide solution was mixed, and pDNA solution was added to the peptide solution; the resultant mixture was mixed immediately and incubated for 15 minutes at room temperature. Then 100µL peptide/pDNA mixture was added to each well and made up to 1mL with growth medium. The plate was gently rocked to ensure that the mixture is evenly distributed. Cells were incubated for 24h before replacing the growth medium, and for a further 24h before end-point analysis. If needed cell were incubated with 10µM SAHA for the first 16h of transfection. If needed cells were treated with 5µM MG132 for 6h before harvest. As explained in Section 3.2, the optimal transfection protocol is suspected to involve treatment with MG132 but without SAHA. Tables [2] and [3] provide representative data of the peptides and pDNA employed in the transfections of this study.

2.2.3 Microscopy Endpoint Analysis:

The medium from the transfection protocol was removed, and the slide washed three times with 0.5mL PBS with 0.1% Tween®20 detergent (PBST). Cells were fixed with either 0.5mL PFA in Phosphate-buffered saline (PBS) at pH 7.4 for 10 minutes at room temperature, or MEth chilled (-20°C) for 5 minutes at room temperature. The fixing agent was then carefully aspirated, the slide washed with ice-cold PBS three times, and if needed the cells were stored in the fridge until needed. PBS was then removed, and the coverslips were mounted on slides. The samples were imaged by confocal microscopy (Zeiss LSM-880®) for zsGreen fluorescence. Images were analysed using the image processing package Fiji®. To assess the percentage of the cell displaying fluorescence while accounting for autofluorescence, test samples were compared with appropriate negative controls.

Peptide	Molecular Weight (g/mol)	Mass per Transfection (µg)	Charge Ratio to 1.00µg pDNA	Volume of 1mM Solution (µL)	Moles ($x10^{-9}$ M)
FLR	5100.25g/mol	8.16	~9.5	1.6	1.6
		16.32	~19	3.2	3.2
FLH	4756.82g/mol	7.61	~5.2	1.6	1.6
		15.22	~10.5	3.2	3.2
		30.44	~21	6.4	6.4

Table [2]: Quantitative Equivalences of Peptide Masses Employed for Transfection
This table shows quantitative data pertaining to the peptide amounts used in transfections

Plasmid	Concentration (ng/ µL)	Volume for 1.00µg pDNA (µL)	Size (bp)	RMM ($\times10^{6}$ g/mol)	Moles per 1.00µg pDNA ($\times10^{-13}$ mol)
pGM-zsGreen	1492	0.670	2801	1.85	5.41
pGM-F-H-ATM	1591	0.629	11324	7.47	1.34
pGM-F-H-MiniATM	1871	0.534	2864	1.89	5.29
pGM-zsGreen-F-H-ATM	1397	0.716	12022	7.93	1.26
pGM-zsGreen-F-H-MiniATM	1670	0.599	3614	2.39	4.18
pGM-zsGreen-T2A-F-H-ATM	1397	0.716	12098	7.98	1.25
pGM-zsGreen-T2A-F-H-MiniATM	2076	0.482	3638	2.40	4.17

Table [3]: Quantitative Analysis of pDNA Stocks
The table provides representative concentrations for the plasmids used in this study, alongside the volumes needed to obtain 1.00µg pDNA of each for transfection

2.2.4 Microscopy Immunoassay:

The protocol was the same as for microscopy zsGreen analysis, up until the removal of PBS after fixing. If PFA was used as the fixing agent, cells were permeabilised by incubation for 10 minutes in PBS containing 0.2% triton X-100, and then washed in PBS three times for 5 minutes each. This permeabilisation step was not conducted when MEth was used as the fixing agent. Cells were incubated for 30 minutes in 0.5mL PBST containing 1% w/v bovine serum albumin (BSA) and 22.52 mg/ml glycine. Cells were washed three times for 5 minutes each in PBST, and incubated in PBST + 1% BSA + 1:500 primary antibody overnight at 4°C. The primary antibody was then decanted, and the cells washed three times in PBS for 5 minutes each. Cells were incubated for 1h at room temperature in PBST + 1%BSA + 1:1000 secondary antibody + 1:2000 Hoechst® stain in the dark. The secondary antibody was then removed, and the cells washed three times in PBS for 5 minutes each in the dark. The coverslips were mounted on slides, and imaged by confocal microscopy (Zeiss LSM-880®) for fluorescence of the fluorophore attached to the secondary antibody. Images were analysed using the image processing package Fiji®. To assess the percentage of the cell displaying fluorescence while accounting for autofluorescence, test samples were compared with appropriate negative controls.

2.2.5 Flow Cytometry Endpoint Analysis:

The process was conducted as microscopy endpoint analysis, with slight variations. After MG132 incubation, HeLa cell were washed three times for 5 minutes with PBS. Then 250µl trypsin was added to each well and incubated for 3 minutes. The digest was transferred to a microfuge tube, and growth medium added in 1:1 ratio with trypsin and mixed. Cells were fixed in either PFA or MEth as described above, centrifuged at 500xg for 5 minutes to remove the fixing agent, re-suspended in ice-cold PBS, and stored in the fridge until needed. Samples

were finally analysed by the flow cytometer (Astrios® EQ) for zsGreen fluorescence, and the data processed using the software package Kaluza®. To account for autofluorescence and assess the percentage of the resulting population with shifted fluorescence, a threshold was arbitrarily set on the fluorescence histogram of the negative control to include less than 1% of cells as signalling positive. The percentage of shifted cells in each test sample was then determined using the threshold of its corresponding negative control.

2.2.6 Flow Cytometry Immunostaining:

The process was conducted as for the flow cytometry endpoint analysis up until storage in the fridge, and then continued as per the microscopy immunoassays. For transitioning between any of the immunostaining steps, HeLa cells were washed once for 5 minutes, incubated with reagents for the prescribed time period, centrifuged at 500xg for five minutes, and disposed of supernatant. After removal of the secondary antibody and washing, cells were resuspended in PBS. They were then analysed by the flow cytometer (Astrios® EQ) for Alexa Fluor®-647 fluorescence, and the data processed using the software package Kaluza®. The populations were analysed for the percentage of shifted cells, as described in Section 2.2.5.

Chapter 3

Results

Results

3.1 Optimisation of GET Peptide : pDNA Mass Ratio:

Transfection efficiency of nanoparticles depends on their physicochemical properties, which in turn is determined by their composition. GET nanoparticles in this study consist of pDNA directly complexed with FLR and FLH. One key aspect of composition is the relative content of GET peptides and pDNA in the formulation, which is assessed in terms of peptide : pDNA mass ratio (PDMR). Increasing the PDMR may enhance transfection efficiency because it corresponds to an elevation in the charge ratio, which in turn increases the overall number of interactions between pDNA and GET peptides. This may enhance the interaction each plasmid forms with the peptides, thereby stabilising the nanoparticles and enhancing GET-mediated uptake (75). This section investigates whether such a positive correlation between PDMR and transfection efficiency applies to the delivery of ATM pDNA in HeLa cells.

HeLa cells were transfected and analysed by flow cytometry as described in Chapter 2. The constructs tested were negative control (no plasmid), positive control (pGM-zsGreen), pGM-zsGreen-F-H-ATM, pGM-zsGreen-F-H-MiniATM, pGM-zsGreen-T2A-F-H-ATM and pGM-zsGreen-T2A-F-H-MiniATM. Three sets of transfections were conducted for each construct, each employing one of the top three formulations described in Table [4]. These were termed Elevated FLR Formulation (ERF), Elevated FLH Formulation (EHF), and Elevated FLR/FLH Formulation (ERHF). ERF was formulated by complexing 16.32µg FLR with 1.00µg pDNA, whereas EHF was formulated by complexing 30.44µg FLH with 1.00µg pDNA. ERHF was formulated by complexing 16.32µg FLR, 15.22µg FLH and 1.00µg pDNA. Cells were treated with 10µM SAHA. Results are also provided for the formulation with unelevated PDMRs in the unpublished report of Branter et al that resulted in the greatest transfection efficiency under similar conditions, so as to provide a comparative baseline that enables establishing the effects of PDMR elevation (95). This formulation is termed the Baseline Formulation (BF), and was formulated by complexing 8.16µg FLR, 7.61µg FLH and 1.00µg pDNA (95).

Formulation	PDMR	Charge Ratio
ERF	16.32µg FLR : 1.00µg pDNA	FLR: 19
EHF	30.44µg FLH : 1.00µg pDNA	FLH: 21
ERHF	16.32µg FLR : 15.22µg FLH : 1.00µg pDNA	FLR: 19 / FLH: 10.5
BF	8.16µg FLR : 7.61µg FLH : 1.00µg pDNA	FLR: 9.5 / FLH: 5.2

Table [4]: Compositions of Elevated PDMR Formulations
This table highlights the quantitative compositions of the Baseline and Experimental Formulations. Each formulation was made up to 100µL with OptiMEM as described in Section 2.2.2. Results for the BF formulation are adapted from the unpublished report of Branter et al (95), to provide a comparative baseline for the assessment of the effects of PDMR elevation.

Table [5] and Figure [7] compare the efficiencies of these transfections, whereas Figure [8] shows the flow cytometry results of the ERF, EHF and ERHF formulations. Care should be taken in the interpretation of these results, as the experiments have not been repeated to enable meaningful statistical analysis. Furthermore, only four formulations were compared. This precludes the derivation of a general trend that links PDMR and GET transfection efficiency over a broad range, that would otherwise extend in applicability beyond the PDMR values examined here. The negative controls did not result in significant signals, whereas the positive controls resulted in high signals. This validates the utility of zsGreen fluorescence and flow cytometry in assessing transgene expression.

Plasmid	BF	ERF	EHF	ERHF
Negative Control (No plasmid)	0.12%	0.33%	0.14%	0.21%
Positive Control (pGM-zsGreen)	96.20%	67.27%	39.18%	74.20%
pGM-zsGreen-F-H-MiniATM	10.96%	34.69%	43.12%	33.60%
pGM-zsGreen-T2A-F-H-MiniATM	24.25%	53.88%	44.18%	60.16%
pGM-zsGreen-F-H-ATM	8.45%	6.99%	8.22%	11.63%
pGM-zsGreen-T2A-F-H-ATM	9.35%	15.05%	20.07%	22.85%

Table [5]: Transection Efficiencies with PDMR Elevation
This table shows the observed transfection efficiencies in HeLa cells, as assessed by zsGreen fluorescence. Cells were transfected with 1.00µg pDNA and the indicated amounts of GET peptides, and treated with 10µM SAHA. N=1 for all figures. Results for the BF formulation are adapted from the unpublished report of Branter et al (95), to provide a comparative baseline for the assessment of the effects of PDMR elevation.

Results suggest that transfection efficiency of each plasmid is significantly higher with ERHF than with BF. This suggests that doubling the PDMR of each peptide in formulations that combine FLR and FLH significantly enhances transfection efficiency. The only exception is the positive control, for which transfection efficiency markedly falls. The general trend suggests that transfection efficiency positively correlates with PDMR, at least within the PDMR ranges employed. Results for the transfection of pGM-zsGreen-T2A-F-H-ATM with ERHF in Table [5] suggest that GET transfection efficiencies exceeding 20% may be feasible for ATM pDNA in HeLa cells.

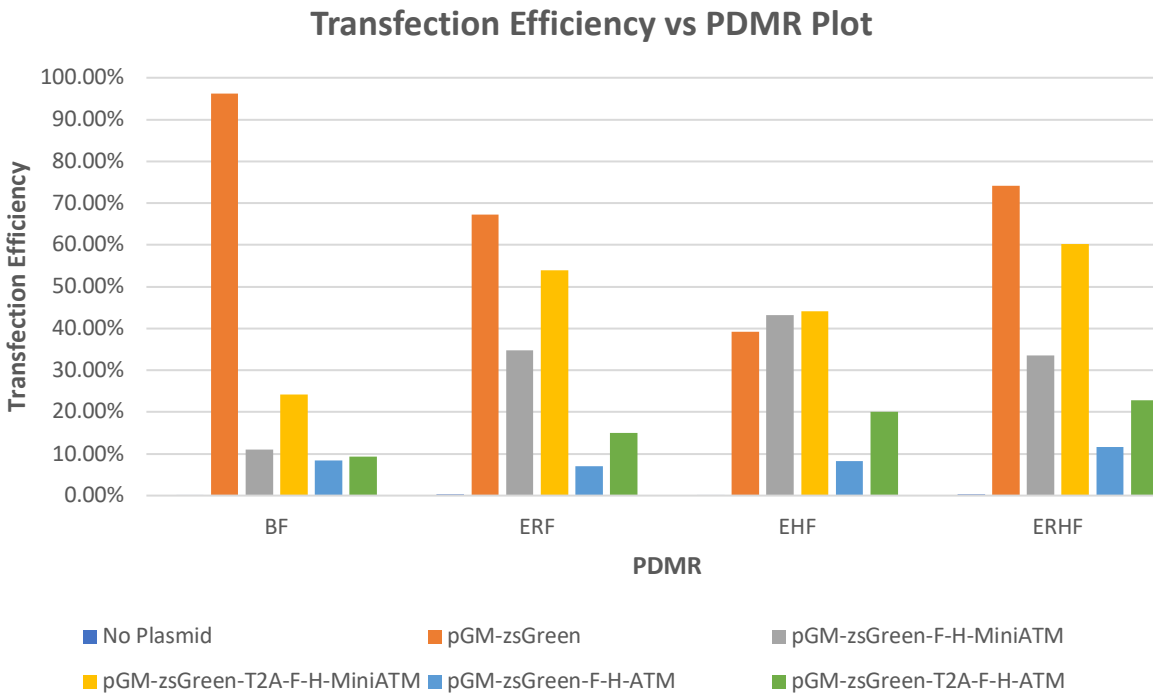


Figure [7]: Transection Efficiency vs PDMR Plot
This figure is a graphical representation of the data in Table [5]. It shows observed transfection efficiencies in HeLa cells, as assessed by zsGreen fluorescence. Cells were transfected with the indicated PDMRs, and treated with 10μM SAHA. N=1 for all figures. Results for the BF formulation are adapted from the unpublished report of Branter et al (95)

Results also indicate a general trend wherein transfection efficiency is higher with ERHF, than with either ERF or EHF. The suggests that at elevated PDMRs, the use of the FLR/FLH combination results in higher transfection efficiency than the use of either peptide alone. This highlights that the synergy of FLR and FLH persists at elevated PDMRs.

Results also show that transfection efficiency of each plasmid is generally higher with either ERF or EHF, than with BF. This indicates that the use of either peptide at an elevated PDMR generally results in higher transfection efficiency, than the use of both at baseline PDMRs. This trend does not apply to the positive control and pGM-zsGreen-F-H-ATM, as transfection efficiency decreases with the former and remains almost unaltered with the latter. The general trend suggests that PDMR better contributes to transfection efficiency than FLR/FLH synergy.

Comparisons can also be made between the transfection efficiencies mediated by ERF and EHF. Results suggest that transfection efficiency of ATM constructs is slightly higher with EHF, perhaps indicating that FLH-mediated endosomal escape is highly relevant to their delivery. This suggests that endosomal escape may be a particularly significant barrier to the delivery of large constructs. One implication of this interpretation is that increasing the relative content of FLH in the formulation may enhance the endosomal escape capacity of the nanoparticle, thereby improving expression of such constructs. Higher transfection efficiencies can be achieved with ERF for smaller constructs, as seen with pGM-zsGreen-T2A-F-H-MiniATM. Smaller constructs may be inherently more susceptible to endosomal escape than larger ones. Sheer uptake by elevated-PDMR FLR thus may be more relevant to enhancing transfection efficiency than the increased endosomal escape activity of elevated-PDMR FLH.

The results can also be used to compare transfection efficiencies of the various plasmids. When conditions are kept uniform, transfection efficiency of the pGM-zsGreen-F-H-ATM construct is consistently lower than that of the smaller construct pGM-zsGreen-F-H-MiniATM.

Likewise, the transfection efficiency of the pGM-zsGreen-T2A-F-H-ATM construct is consistently lower than that of the smaller construct pGM-zsGreen-T2A-F-H-MiniATM. As the amount of pDNA used is 1.00 μg regardless of molecular mass, the lower transfection efficiency of larger plasmids may be attributed to the lower number of moles employed. Alternatively, there may be a negative correlation between transfection efficiency and transgene size. Assessing the extent to which each explanation contributes to transfection variations requires further experimentation.

Under similar conditions, transfection efficiencies of T2A-fusion plasmids are consistently greater than those of their direct-fusion counterparts. This is observed by comparing pGM-zsGreen-T2A-F-H-MiniATM with pGM-zsGreen-F-H-MiniATM, and by comparing pGM-zsGreen-T2A-F-H-ATM with pGM-zsGreen-F-H-ATM. These results suggest that fluorescence may be compromised when zsGreen is permanently fused to the ATM protein, due to such factors as co-degradation or unfavourable interaction between the two proteins. The use of T2A-linked fusions therefore may be better estimate actual transfection efficiency.

When all these results are taken together, an overall interpretation of the relationship between PDMR and transfection efficiency can be drawn. Transfection efficiency mediated by the combination of GET peptides at elevated PDMRs (ERHF) is greater than that of either peptide alone at an elevated PDMR (ERF and EHF), which in turn is greater than that of both peptides at baseline PDMRs (BF). This can be explained in terms of elevated PDMRs enhancing peptide-pDNA interactions in GET complexes, thereby improving nanoparticle stability and uptake. The PDMR effect appears to better contribute to overall transfection efficiency in isolation than the FLR/FLH synergy does. The FLR/FLH synergy is due to the predominant roles of these peptides in respectively mediating cellular uptake and endosomal escape, which together counter major barriers to transgene expression. This synergy persists at elevated PDMRs. ERHF therefore is associated with optimal transfection efficiencies because it combines this synergy with PDMR elevation of both peptides.

Some exceptions to this general interpretation warrant further analysis. The positive control is a seemingly notable exception, as its transfection efficiency appears to be highest with BF. This plasmid is the smallest among those tested, and therefore may be inherently the most efficiently transfected. This plasmid also has the smallest molar mass of those tested, such that 1.00μg of pDNA corresponds to the greatest number of plasmid copies. Baseline transfection efficiency already exceeds 95%, so further enhancements due to PMDR elevations may result in pDNA over-uptake or over-expression. This in turn may interfere with cell viability, which in turn may skew the measured transfection efficiency. The results thus may not necessarily signify a true exception, and further experimentation is needed to validate this explanation.

The other notable exception is pGM-zsGreen-F-H-ATM, for which ERF and EHF do not significantly alter transfection efficiency when compared with BF. This can be explained as a combination of two reasons. First, its large size can significantly interfere with transfection efficiency. As the activities of FLR and FLH are respectively better tailored to mediate uptake and endosomal escape, the employment of either peptide alone may be insufficient to achieve observable expression gains even at an elevated PDMR. This explanation is supported by the observation that the general trend does apply to the smaller pGM-zsGreen-F-H-MiniATM plasmid. Second, the fluorescence efficiency of zsGreen may be reduced owing to its direct coupling to the intact ATM protein, which is tightly regulated. Relatively small improvements in transfection efficiency, such as those mediated by the use of a single peptide at an elevated PDMR, may be masked. This is evidenced by the fact that pGM-zsGreen-T2A-F-H-ATM complies with the general trend. T2A linkage and/or FLH/FLR synergy are therefore needed with PDMR elevation to significantly increase observable transfection efficiency of ATM.

In conclusion, limited evidence is provided that suggests PDMR positively correlates with transfection efficiency. The highest transfection efficiency is achieved with the use of the FLR/FLH combination at elevated PDMRs. It may be able to mediate transfection efficiencies exceeding 20% for ATM pDNA in HeLa cells.

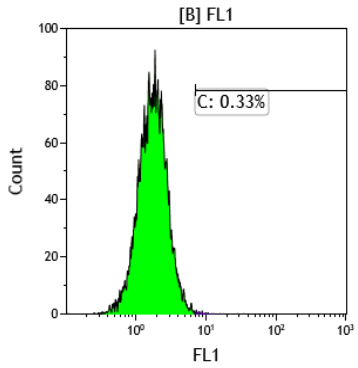
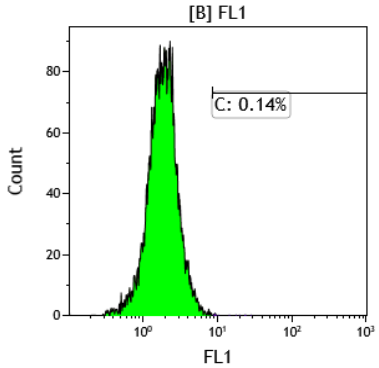
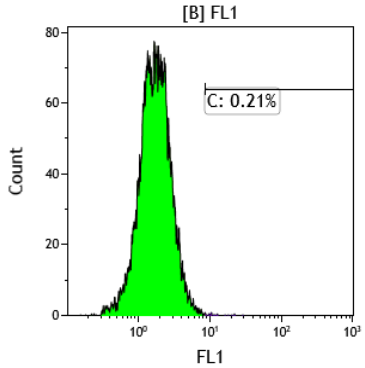
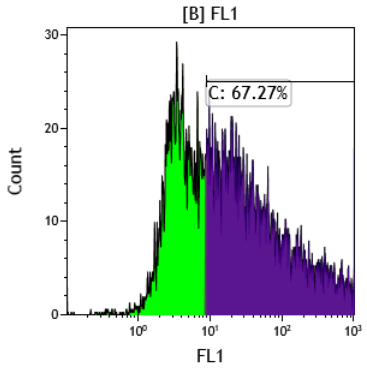
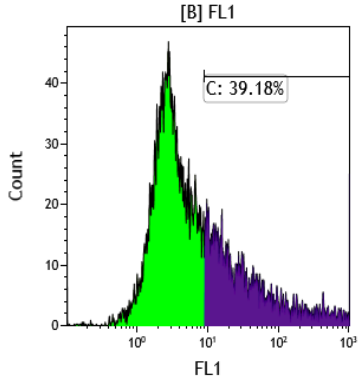
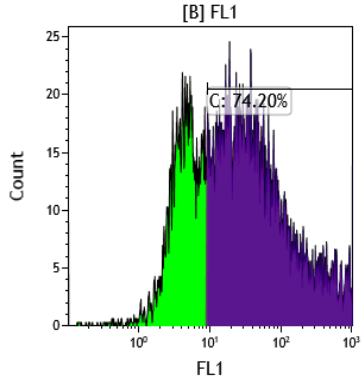
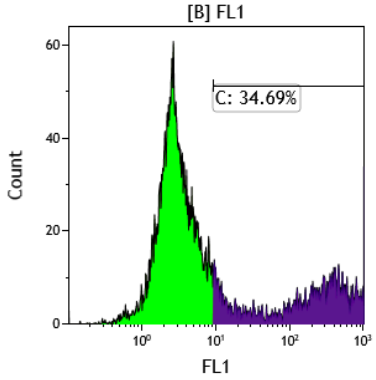
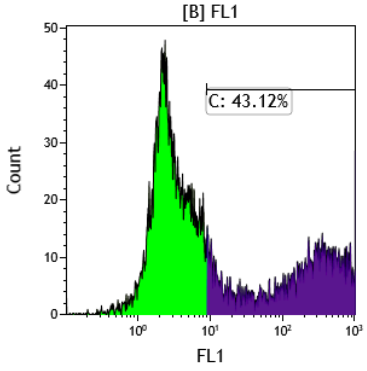
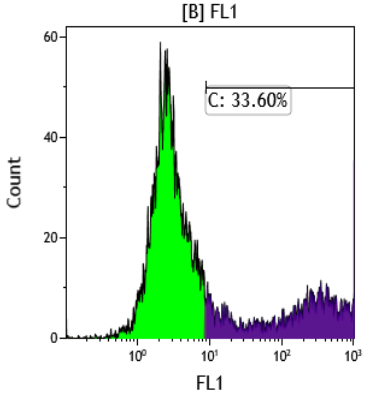
Plasmid	ERF	EHF	ERHF
Negative Control (No plasmid)			
Positive Control (pGM-zsGreen)			
pGM-zsGreen-F-H-MiniATM			

Figure [8]: Flow Cytometry Analysis for PDMR Elevation

This figure shows flow cytometry analysis for zsGreen fluorescence following transfection of 100,000 HeLa cells with 1.00µg pDNA and the indicated amounts of GET peptides, which correspond to elevated PDMRs. Cells were treated with 10µM SAHA. Figure is continued below.

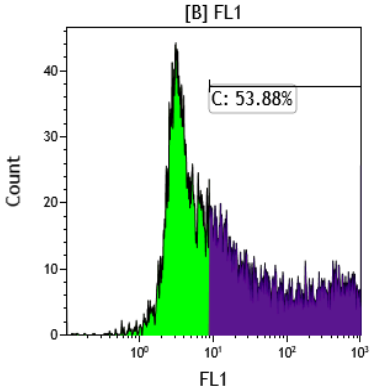
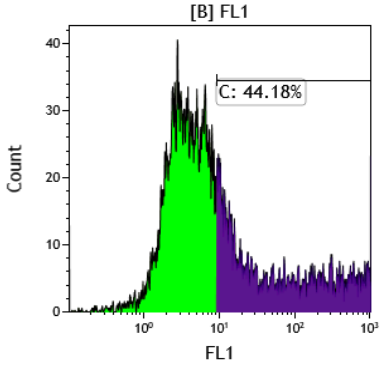
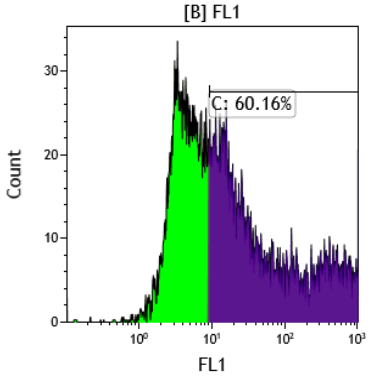
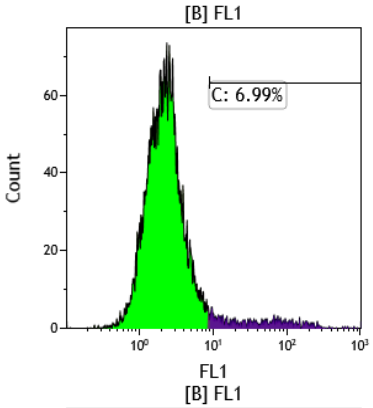
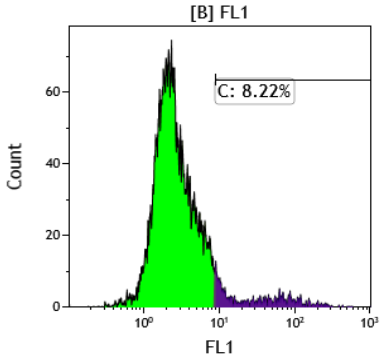
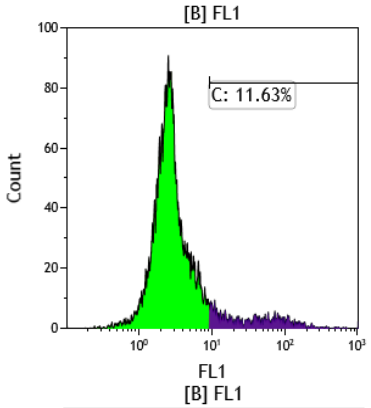
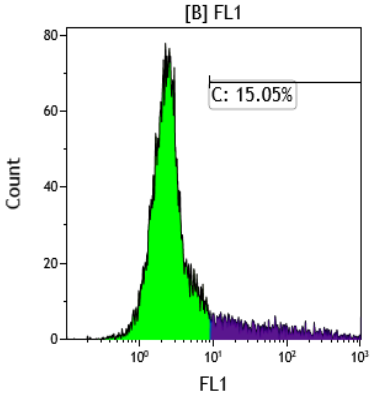
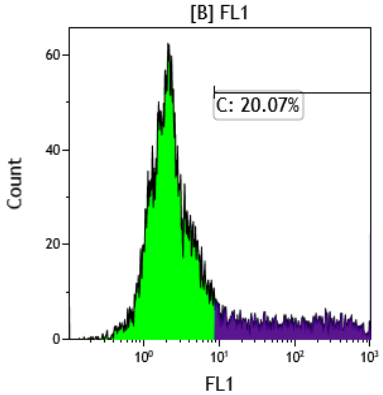
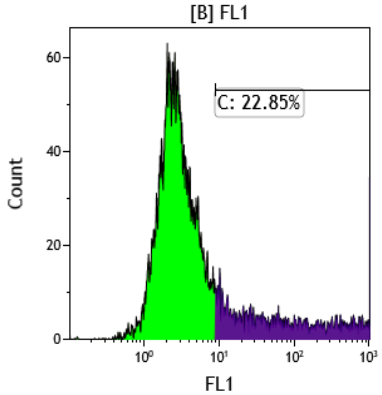
Plasmid	ERF	EHF	ERHF
pGM-zsGreen-T2A-F-H-MiniATM			
pGM-zsGreen-F-H-ATM			
pGM-zsGreen-T2A-F-H-ATM			

Figure [8]: Continued from above.

3.2 Optimisation of ATM Stabilisation Regimen:

Due to its complex functions and interactions, ATM expression is tightly regulated as discussed in Section 1.2. Such regulation may interfere with expression of transfected ATM, thereby underestimating transfection efficiency. Experiments in Section 3.1 employed the histone deacetylase inhibitor SAHA to stabilise ATM expression. MG132 stabilises ATM expression by a different mechanism, namely by interfering with the degradation of ATM protein to increase its intracellular half-life (68). It can therefore be investigated as a stabilising agent to substitute or complement SAHA. The aim of this section is thus to optimise the ATM stabilisation regimen, by characterising the transfection efficiencies observed with MG132 treatment.

HeLa cells were transfected and analysed for zsGreen fluorescence by endpoint flow cytometry as described in Chapter 2. The constructs tested were negative control (no plasmid), positive control (pGM-zsGreen), pGM-zsGreen-F-H-ATM, pGM-zsGreen-T2A-F-H-ATM and pGM-zsGreen-T2A-F-H-MiniATM. The transfection complex consisted of 1.00µg pDNA, 16.32µg FLR and 15.22µg FLH. Three experimental sets were compared for each construct. The first was treated with 10µM SAHA, and is the same as the ERHF sample tested in Section 3.1. The second was treated with 5µM MG132, and third with both 10µM SAHA and 5µM MG132.

Table [6] and Figure [9] compare transfection efficiencies of the treatment regimens employed, whereas Figure [10] shows the experimental flow cytometry results. In short, treatment with 5µM MG132 alone results in the greatest transfection efficiencies for all plasmids. Treatment with both agents results in greater transection efficiencies than treatment with 10µM SAHA alone for most plasmids, the exception being pGM-zsGreen-F-H-ATM. The result for pGM-zsGreen-T2A-F-H-ATM in Table [6] indicates that GET transfection efficiencies around 50% may be feasible for ATM pDNA in HeLa cells.

Plasmid	Experimental Set 1	Experimental Set 2	Experimental Set 3
	10µM SAHA No MG132	**10µM SAHA 5µM MG132**	**No SAHA 5µM MG132**
Negative Control (No plasmid)	0.21%	0.65%	0.84%
Positive Control (pGM-zsGreen)	74.20%	83.81%	95.56%
pGM-zsGreen-F-H-ATM	11.63%	8.99%	26.89%
pGM-zsGreen-T2A-F-H-ATM	22.85%	44.33%	48.92%
pGM-zsGreen-T2A-F-H-MiniATM	60.16%	67.95%	82.20%

Table [6]: Transfection Efficiencies with 5µM MG132 and/or 10µM SAHA Treatment
This table shows the observed transfection efficiencies of the plasmids indicated in HeLa cells, as assessed by zsGreen fluorescence. Cells were transfected with 1.00µg pDNA, 16.32µg FLR, and 15.22µg FLH. They were treated with 10µM SAHA, 5µM MG132, or both as indicated. N=1 for all figures.

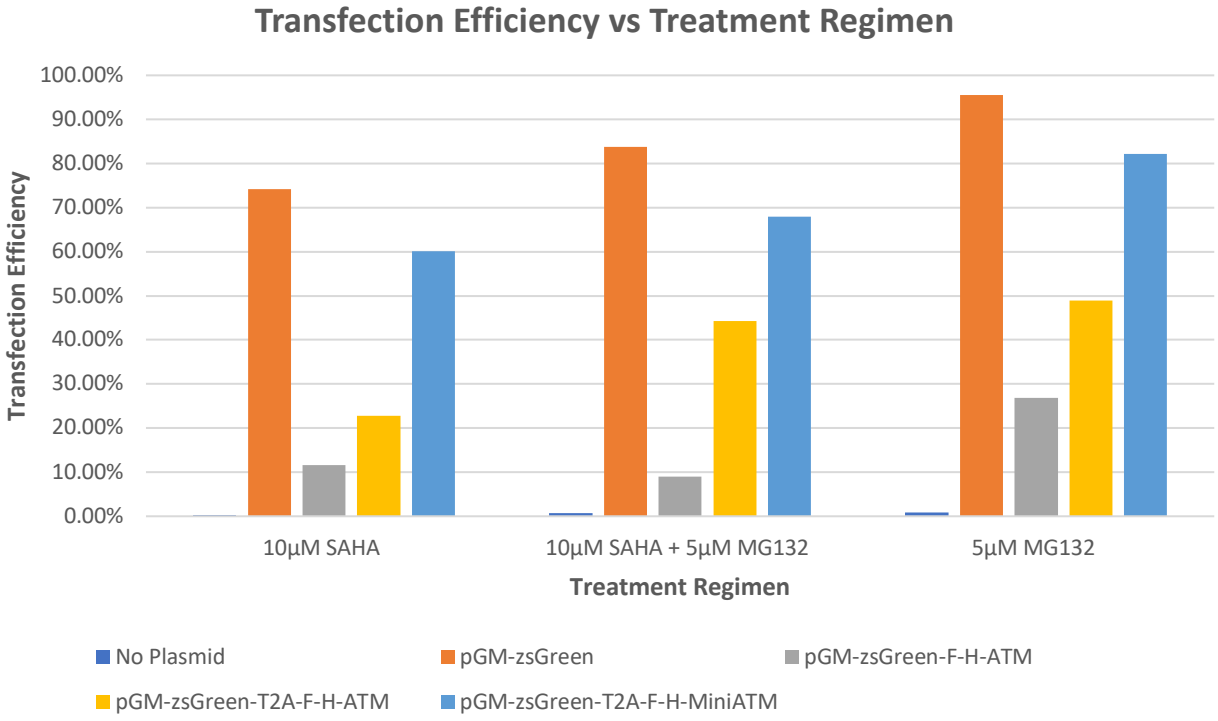


Figure [9]: Transection Efficiency vs Treatment Regimen Plot
This figure is a graphical representation of the data in Table [6]. It shows observed transfection efficiencies in HeLa cells, as assessed by zsGreen fluorescence. Cells were transfected with 1.00µg pDNA, 16.32µg FLR, and 15.22µg FLH, and treated with the indicated regimens. N=1 for all figures.

Care should be taken in the interpretation of these results, as they are associated with several limitations. This experiment has not been repeated sufficiently for reproducibility analysis, so it is impossible to decisively confirm the statistical robustness of the observed increase in transfection efficiency. MG132 has been reported in the literature to induce dose-dependent apoptosis and growth arrest in HeLa cells, with an IC_{50} for the latter effect of 5μM for 24 hour incubation (101). Due to the gating employed in flow cytometry analysis, the results obtained may not be representative of the entire transfected population. Furthermore, any potential effects of ATM expression on inhibiting MG132-mediated apoptosis and growth arrest have not been characterised yet. The use of zsGreen fluorescence does not allow the direct detection of ATM protein, rendering it impossible to directly analyse the effects of SAHA or MG132 treatments on its intracellular concentration. MG132 is reported in the literature to inhibit degradation of fluorescent proteins (102). It therefore could be the case that MG132-mediated enhancements in fluorescence signals are due to stabilisation of zsGreen. The extent to which such stabilisation of zsGreen correlates with that of ATM protein is unknown.

To interpret these results, it would be worthwhile to compare each experimental set to the others. Co-treatment with SAHA and MG132 results in greater expression efficiencies than treatment with SAHA alone for most plasmids, thereby validating the stabilising effect that MG132 may have on ATM expression. Treatment with 5μM MG132 stabilises ATM expression to a greater extent than does treatment with 10μM SAHA, suggesting that it is a more effective stabilisation agent. Treatment with MG132 also results in greater transfection efficiencies than co-treatment for all plasmids, thereby precluding synergy between the two agents. This also confirms that SAHA may interfere with transfection and/or expression efficiencies, thereby reducing expression gains achieved by MG132 treatment alone.

Several possible explanations exist as to why MG132 may be a more effective stabilising agent than SAHA. The first is that rapid proteasomal degradation may be a more significant limiting

factor to the kinetics of ATM protein levels, than is transgene expression. The second explanation is that SAHA may interact unfavourably with GET peptides in a yet uncharacterised manner, whereas MG132 may not have such an effect. A third explanation is based on the fact that SAHA treatment overall stabilises ATM proteins in cancerous cell lines, but may have an inhibitory effect on ATM expression that is prominent in transformed cell lines (103). It could be that SAHA also has a residual inhibitory effect in cancerous cell lines, which is masked by its stabilising effect. MG132 in contrast may not have such an inhibitory effect, thereby leading to greater overall ATM stabilisation. The aforementioned second and third explanations can also elucidate why MG132 treatment better stabilises ATM expression than co-treatment regimens. SAHA's interactions with GET peptides and residual inhibitory effects on ATM expression may counter gains in expression efficiency from MG132 treatment.

It may be relevant to compare the results of this section, with those of unpublished work of Branter et al presented in Section 1.7 (95). The latter results have found treatment with 10μM SAHA alone to mediate better ATM stabilisation than co-treatment with 5μM MG132 (95). One explanation is that the work of Branter et al did not incorporate optimal transfection conditions. For example, the constructs they tested were devoid of T2A linkage, and GET peptides were not employed at elevated PDMRs (95). Such improvements may have therefore been necessary to demonstrate benefits of MG132 treatment.

In conclusion, the optimal stabilisation regimen appears to consist solely of treatment with 5μM MG132. GET transfection efficiencies up to 50% may be achievable for ATM pDNA in HeLa cells.

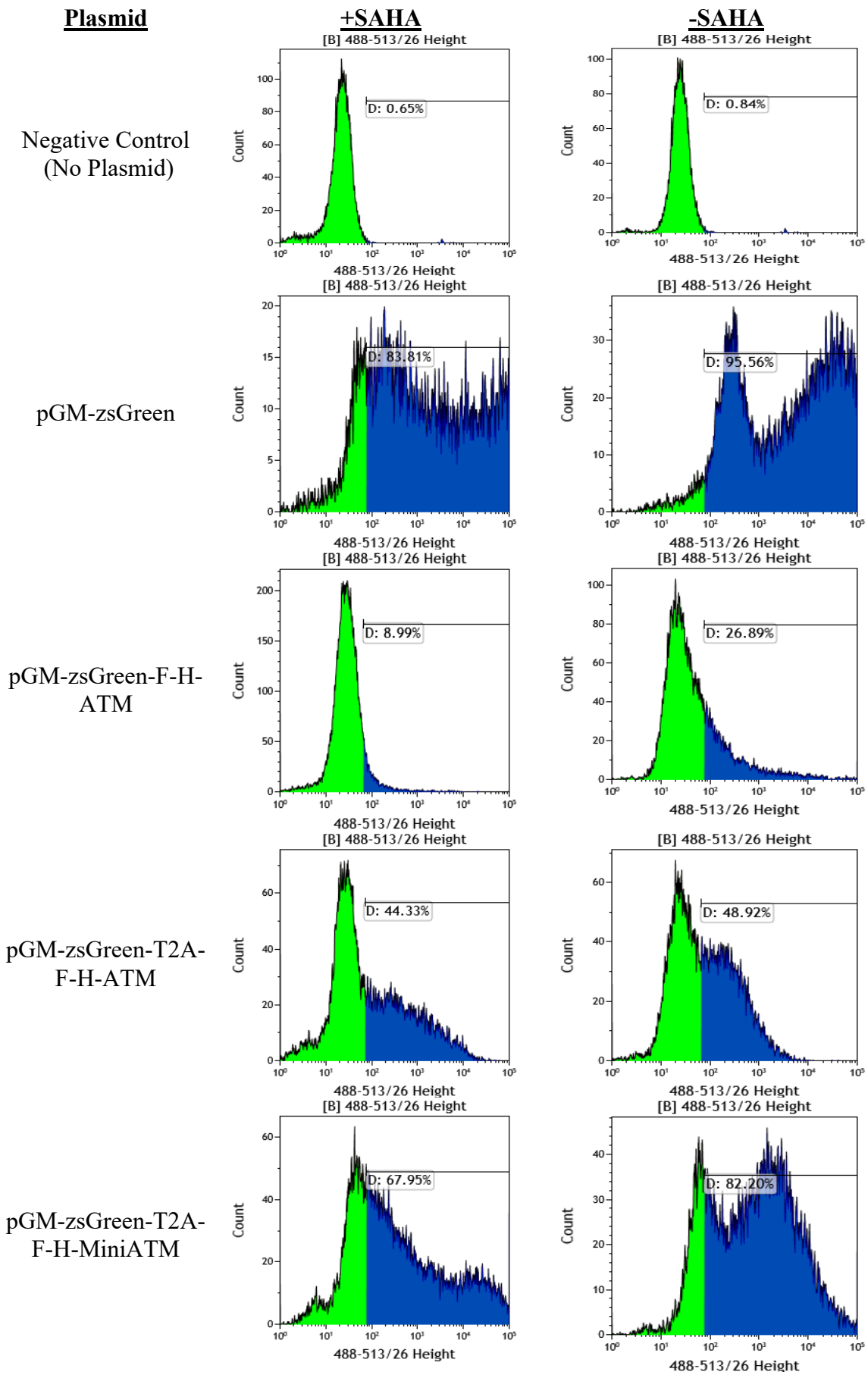


Figure [10]: Flow Cytometry Analysis for 5µM MG132 and/or 10µM SAHA Treatment
This figure shows experimental flow cytometry analysis for zsGreen fluorescence following transfection of 100,000 HeLa cells with 1.00µg pDNA, 16.32µg FLR, and 15.22µg FLH. Cells were treated with 5µM MG132, either with or without co-treatment with 10µM SAHA.

3.3 Analysing Transfection Efficiency by Immunostaining:

Immunostaining, as discussed in Section 1.4, is a technique commonly used to establish protein expression. It offers several advantages, as it would enable direct detection, analysis and localisation of ATM protein. This contrasts with the zsGreen fluorescence assay, which relies on the surrogate measure of a reporter protein's fluorescence to indicate transgene expression. ATM primary antibodies lack adequate specificity. ATM in immunocytochemistry assays of this thesis is therefore conjugated with a flag tag, for which specific primary antibodies are commercially available. This section therefore aims to establish expression of transfected ATM via immunostaining, with the results analysed by both confocal microscopy and flow cytometry. It also aims to compare the results obtained by immunostaining and zsGreen fluorescence assays, to confirm their matching.

HeLa cell samples were transfected and analysed as described in Chapter 2. The constructs examined were negative control (pGM-zsGreen), pGM-zsGreen-F-H-MiniATM, pGM-zsGreen-T2A-F-H-MiniATM, pGM-zsGreen-F-H-ATM and pGM-F-H-ATM. All transfections employed 1.00μg pDNA, 16.32μg FLR and 15.22μg FLH. All samples were treated with 5μM MG132, and immunostained with the primary and secondary antibodies. Samples were analysed for both zsGreen and AlexaFluor-647 fluorescences, respectively by endpoint and immunostaining microscopies.

Microscopic results of one immunostaining experiment are shown in Figure [11]. They are inconsistent with those of zsGreen fluorescence, as assessed by flow cytometry in Sections 3.1 and 3.2. The immunostaining microscopy results for example suggest that transfection efficiencies are ubiquitous and uniform across plasmids. These respectively contradict the limited and plasmid-dependent transfection efficiencies observed with zsGreen fluorescence in flow cytometry assays. This raised initial suspicions the secondary antibody may be non-specifically binding to intracellular components.

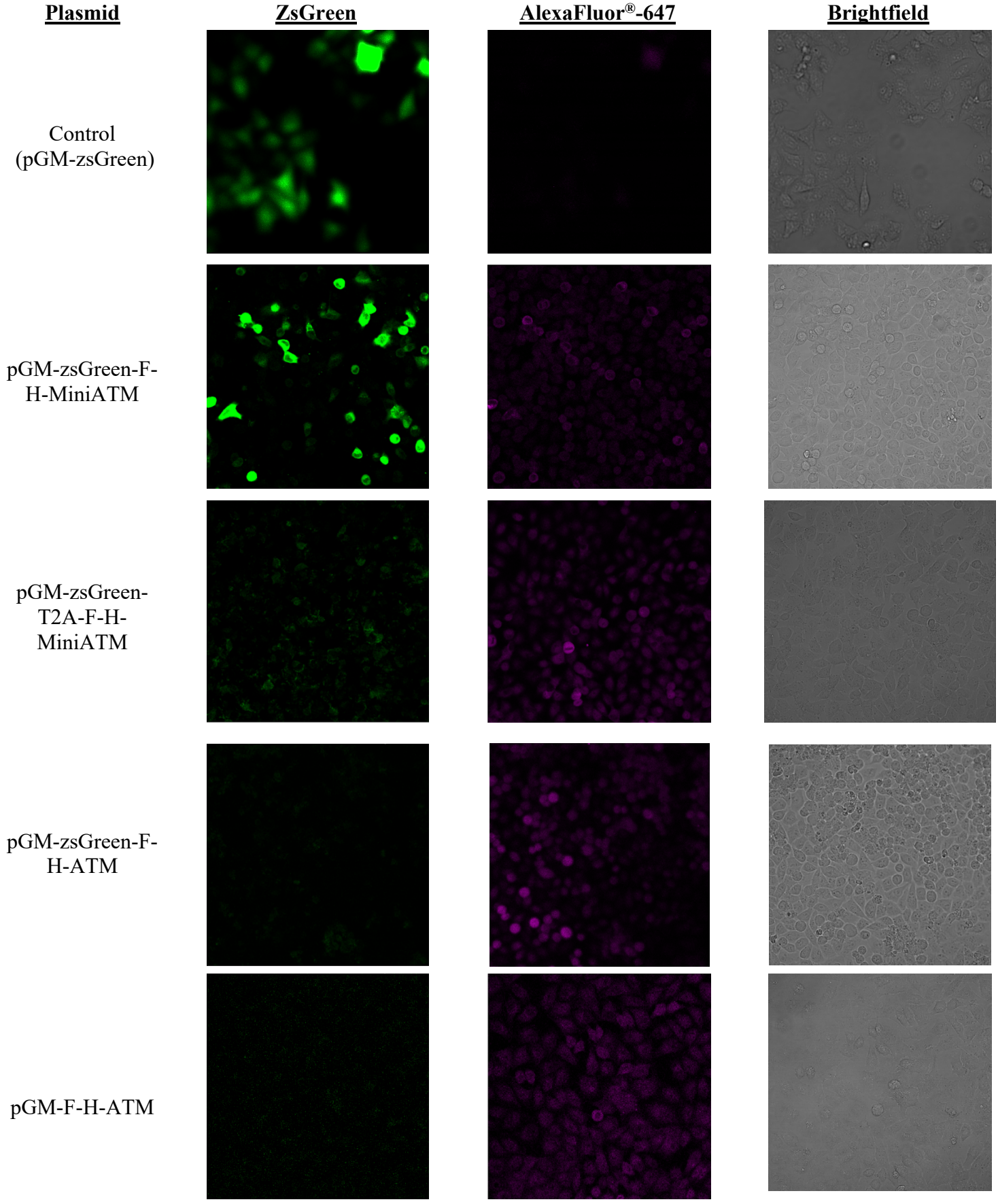


Figure [11]: Microscopic Analysis for 5µM MG132 Treatment
This figure shows microscopic analysis for zsGreen fluorescence (zsGreen) and immunostaining (AlexaFluor®-647) following transfection of HeLa cells with 1.00µg pDNA, 16.32µg FLR and 15.22µg FLH. Cells were treated with 5µM MG132, and stained with the primary and secondary antibodies.

Analysis of zsGreen fluorescence by microscopy also rendered inconsistent results. Fluorescence efficiency with pGM-zsGreen-T2A-F-H-MiniATM for example appears with microscopy to be less than that with pGM-zsGreen-F-H-MiniATM. This contradicts flow cytometry findings in Sections 3.1 and 3.2, which indicate that T2A linkage enhances observed transfection efficiency. Fluorescence with pGM-zsGreen-F-H-ATM was indistinguishable from that of pGM-F-H-ATM, despite the latter not encoding zsGreen. This again contradicts the analysis of zsGreen fluorescence by flow cytometry, which suggests a transfection efficiency for pGM-zsGreen-F-H-ATM exceeding 20% as seen in Figure [10]. Differences between microscopy and flow cytometry assays may account for some of these result variations. The latter is more sensitive to signal detection than microscopy, and renders more objective results (104). Another notable difference is that flow cytometry results are based on gated analyses of suspended samples, whereas microscopic ones are based on ungated analyses of adherent samples. Permeabilisation, blocking and immunostaining of the microscopic samples may have also contributed to the diverging results. As flow cytometry samples were not immunostained, any interference of the antibodies with zsGreen fluorescence and/or T2A self-cleavage would have only affected the microscopy samples. Transfection of 100,000 and 40,000 cells respectively for flow cytometry and microscopy, using the same amounts of pDNA and peptides, is a final source of variation.

Replications of the experiment provided further evidence for non-specific binding of the secondary antibody. Examples are shown in Figure [12]. Construct pGM-Glux does not contain the flag-tag, but cells transfected with it stained positive. Immunostaining following transfection with construct pCMV-F-H-ATM resulted in a signal distribution that covers the cytoplasmic as well as nuclear compartments, and thus does not correspond to the nuclear localisation of ATM protein.

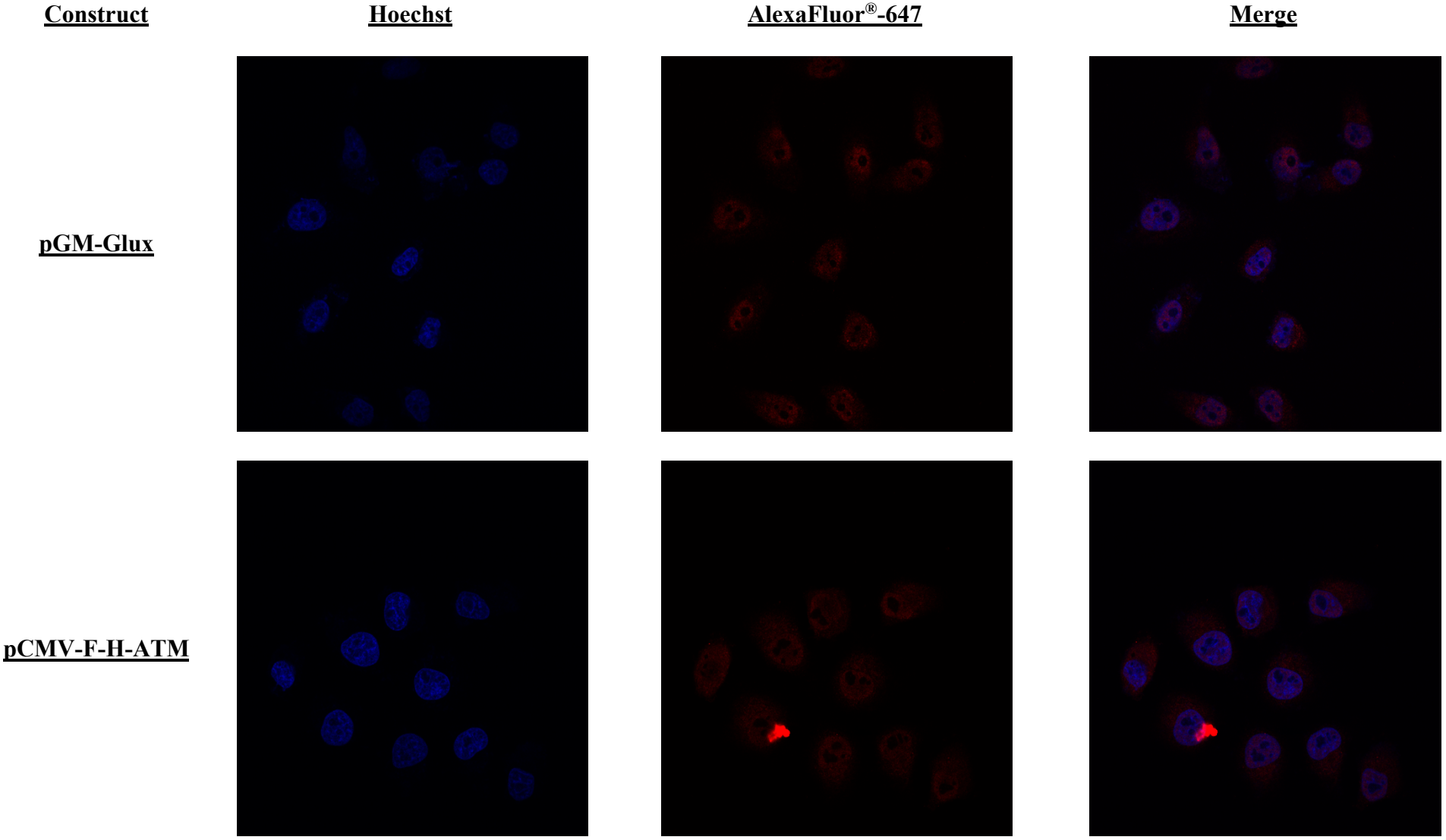


Figure [12]: Microscopic Evidence for Non-Specific Binding of Secondary Antibody
This figure shows microscopic analysis for Hoechst staining and AlexaFluor®-647 immunostaining following transfection of HeLa cells with 1.00µg pDNA, 16.32µg FLR and 15.22µg FLH. Cells were treated with 5µM MG132, and stained with the primary and secondary antibodies. The top row shows positive staining of a negative control that lacks the flag tag. The bottom row shows widespread cytoplasmic immunostaining, which contrasts the nuclear localisation of ATM proteins.

In order to better compare immunostaining results with those of zsGreen fluorescence in Sections 3.1 and 3.2, it was deemed necessary to analyse immunostaining samples with flow cytometry. This would ensure that inherent differences between flow cytometry and microscopy do not contribute to the inconsistencies across experiments. HeLa cells were thus transfected and analysed by flow cytometry immunostaining, as described in Chapter 2. All transfections employed 1.00μg pDNA, 16.32μg FLR and 15.22μg FLH. The constructs tested were first negative control (no plasmid), second negative control (pGM-Glux), positive control (pGM-F-H-MiniATM), pGM-F-H-ATM and pCMV-F-H-ATM. Two sets of transfections were conducted for each construct, one with 5μM MG132 treatment and one without.

These immunostaining flow cytometry results are shown in Figure [13]. All samples either had one peak corresponding to positive staining, or two peaks corresponding to positive and negative staining. This applied to the negative controls. Positive immunostaining of the negative controls provided further evidence for non-specific binding of the secondary antibody, which precluded meaningful interpretation of the results.

Experiments were then conducted to specifically and decisively examine the secondary antibody for non-specific binding. Three samples of HeLa cells were transfected with pGM-F-H-MiniATM, and analysed by flow cytometry immunostaining as described in Chapter 2. The first was not immunostained. The second was immunostained by the secondary antibody alone, and the last by both the primary and secondary antibodies. All transfections employed 1.00μg pDNA, 16.32μg FLR, and 15.22μg FLH. Cells were not treated with SAHA or MG132, to preclude any interference they may have with antibody binding. Two replicas of the experiment were conducted. The first employed MEth solely as the fixing and permeabilising agent, whereas the second employed PFA and Triton X-100 respectively as the fixing and permeabilising agents.

Flow cytometry results for the sample fixed with MEth are shown in Figure [14]. A single negative peak was obtained with the unstained sample as expected. Positive peak shifts were observed after immunostaining with the secondary antibody alone, and with both antibodies. The shifted peak was significantly larger than the negative peak for both samples. Positive immunostaining of the second sample confirms non-specific binding of the secondary antibody. Results for the sample fixed with PFA and permeabilised with Triton X-100 are not shown, as cell recovery was too low for meaningful interpretation.

To summarise findings from these different experiments, reasonable interpretation of immunostaining assays was precluded by the non-specific binding of the secondary antibody. Immunostaining analysis by microscopy first raised suspicions for non-specific binding, as results suggested uniformly high transfection efficiencies for all constructs. Immunostaining analysis by flow cytometry raised similar suspicions, as negative controls stained positive. These suspicions were confirmed by a flow cytometry experiment designed purposely to examine antibody specificity. In the absence of the primary antibody treatment, the majority of cells treated with the secondary antibody in this last experiment stained positive. This verifies that the secondary antibody is likely binding non-specifically to either cellular components or transfection agents. These results are unexpected, as the secondary antibody has been used successfully in published immunostaining studies (50). One possible explanation is a defect in the specific batch employed in this study, which could for example result from disruptions to the cold chain in its lifetime. Alternatively, the secondary antibody may be incompatible with one or more components of the transfection protocol. Finally, such experimental errors as poor blocking or inadequate washings may have amounted to the non-specific signals observed.

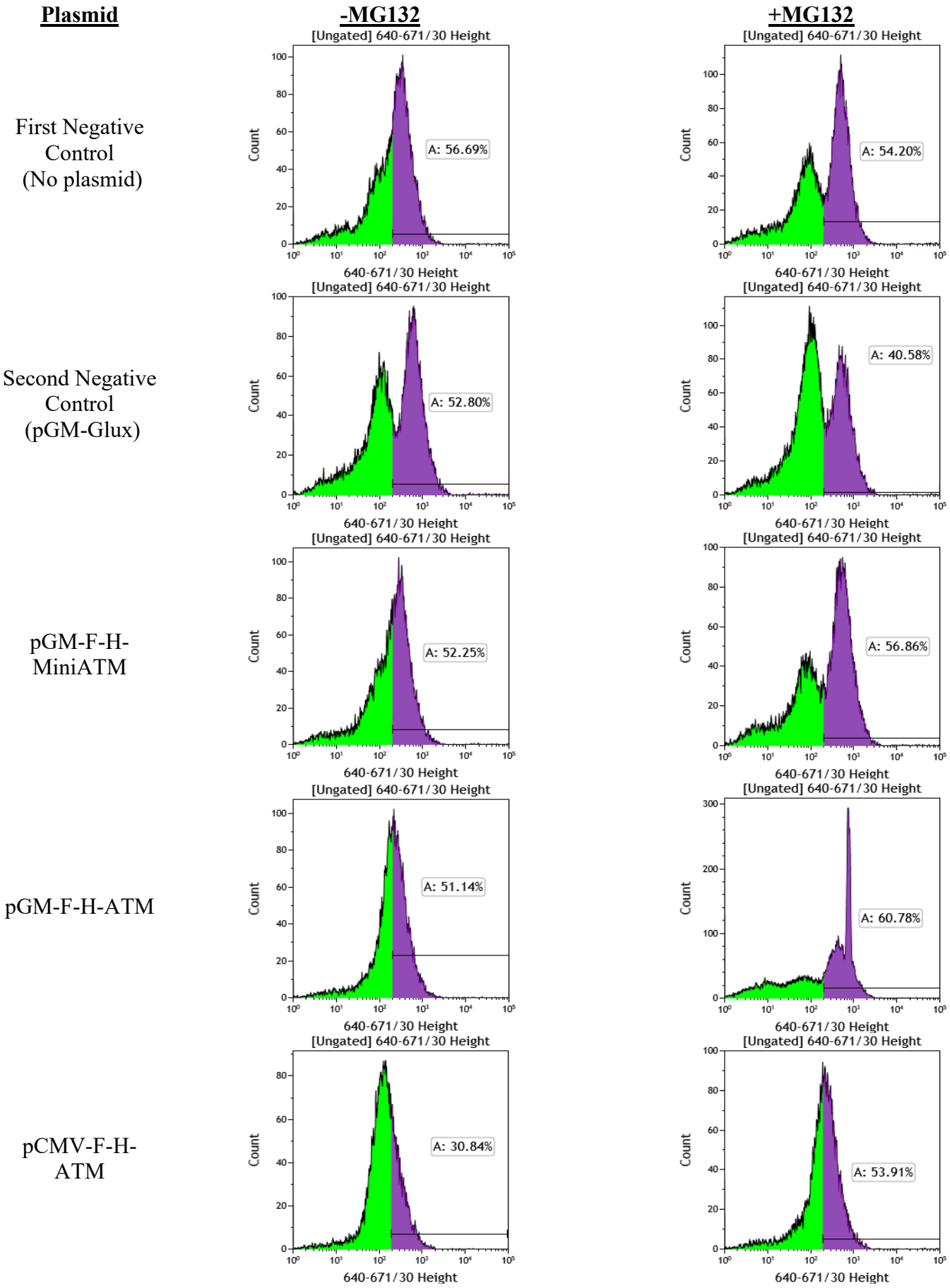


Figure [13]: Flow Cytometry Analysis for 5µM MG132 Treatment
This figure shows flow cytometry analysis for AlexaFluor®-647 fluorescence following transfection of HeLa cells with 1.00µg pDNA, 16.32µg FLR, and 15.22µg FLH. Cells were fixed with PFA, stained with the primary and secondary antibodies, and either treated with 5µM MG132 or not.

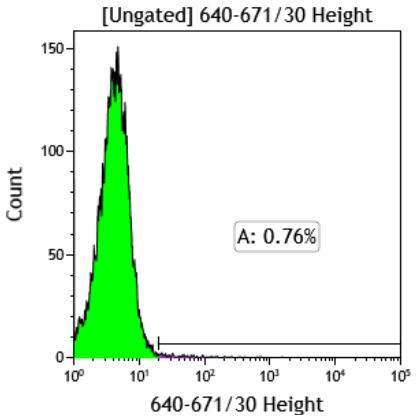
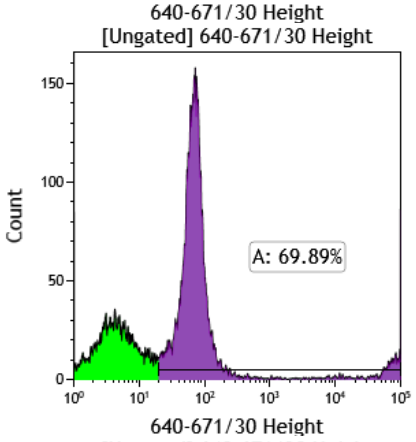
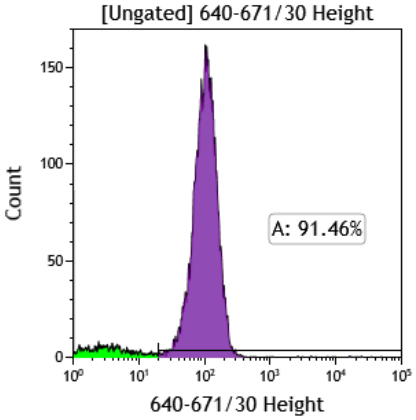
Plasmid	AlexaFluor®-647 Staining
pGM-F-H-MiniATM Primary Antibody – No Secondary Antibody - No	
pGM-F-H-MiniATM Primary Antibody – No Secondary Antibody - Yes	
pGM-F-H-MiniATM Primary Antibody – Yes Secondary Antibody - Yes	

Figure [14]: Flow Cytometry Analysis for Secondary Antibody Specificity
This figure shows flow cytometry analysis for AlexaFluor®-647 fluorescence following transfection of HeLa cells with 1.00µg pDNA, 16.32µg FLR, and 15.22µg FLH. Cells were immunostained as indicated, and fixed with MEth.

The last experiment also examined the optimal cell fixing and permeabilisation regimen, by comparing the MEth and PFA/Triton X-100 protocols. The latter resulted in poor cell recovery for flow cytometry. PFA acts solely as a fixing agent, such that cells require permeabilization by further treatment with Triton X-100. The additional washing step may compromise cell counts in the final sample. MEth on the other hand acts simultaneously as a fixing and permeabilization agent, and therefore bypasses treatment with Triton X-100. Cell recovery with the MEth regimen was sufficient to meaningfully interpret the flow cytometry results.

In conclusion, immunostaining results were inconclusive due to non-specific binding of the secondary antibody.

Chapter 4

Discussion

Discussion

AT is a devastating, progressive and multisystemic disorder that results from loss of function of ATM (1-6). Treatment options are currently limited and palliative, with none having true disease-modifying properties that effectively interfere with prognosis (1-6). Since the disease is monogenic, gene therapy would be the ideal treatment approach. The AT gene therapy project at the University of Nottingham is the first of its kind in attempting to develop a universal non-viral gene therapy for this disorder. This MRes study has attempted to build on previous evidence that points towards the feasibility of employing GET for ATM pDNA delivery. Its results highlight PDMR and MG132 treatment as experimental conditions that could be relevant to optimising transfection efficiency *in vitro*, as assessed by zsGreen fluorescence via flow cytometry. The results are however associated with numerous limitations, including insufficient number of replications and limited range of experimental parameters explored. Experimental limitations have also precluded conclusive detection of expressed ATM protein by immunostaining. This section discusses interpretations of these findings, and elaborates on the limitations that need to be addressed in further developments.

It may be worthwhile to start with providing a general overview of the experimental structure of this thesis, within the context of previous efforts that have been conducted by the group. Branter et al have first identified direct complexation of ATM pDNA with GET peptides as a suitable modality for the purposes of this project (95), which corresponds to the first of three GET gene therapy modalities described in Section 1.6. Branter et al have also demonstrated the relevance of immunostaining, zsGreen fluorescence, flow cytometry, confocal microscopy and SAHA stabilisation to assessing transfection efficiency of ATM pDNA (95). Section 3.1 of this thesis build on these findings by attempting to optimise the formulation of the nanoparticles, in terms of total peptide to pDNA content. Section 3.2 of this thesis attempts to optimise the stabilisation regimen of ATM, and suggests that proteasomal inhibition by MG132

may be more suitable than expression induction by SAHA. Although ATM expression is yet to be confirmed by immunostaining, preliminary evidence by zsGreen fluorescence suggests that *in vitro* transfection efficiencies of ATM pDNA up to 50% may be attainable in HeLa cells.

Before discussing results, it is relevant to provide a critical overview of the methodologies used in this thesis. One technique to evaluate transfection efficiency involves assessment of zsGreen fluorescence via flow cytometry. This approach is technically less demanding than immunostaining, as it does not involve additional preparations beyond transfection. It is also useful to providing early evidence for expression of proteins, for which no specific antibodies are available. Flow cytometry provides a quantitative, objective and sensitive assay to assess changes in fluorescence. These traits make it an appropriate tool for the purposes of this thesis, wherein rapid assessments for transfection efficiency enhancements are desirable. This technique however has the inherent limitation of assessing expression using the surrogate measure of a reporter protein's fluorescence. It does not directly detect the target protein, and as such cannot be used to analyse its intracellular stability, localisation or functionality. The standalone evidence it provides for transfection is therefore inadequate for the purposes of gene therapy studies, and requires supplementation with such methodologies as immunostaining and functionality assays. This assay has confirmed general trends relating to zsGreen fluorescence that were previously noted by Branter et al, including its negative correlation with plasmid size and positive correlation with T2A linkage (95). Despite this apparent general consistency, experiments in this thesis have not been replicated sufficiently to assess statistical robustness. They thus have to be repeated in the future, to assess the reproducibility of this assay's results in determining transfection efficiency of ATM pDNA.

Plasmid size and T2A linkage were identified as factors that may affect zsGreen signalling in the aforementioned flow cytometry assay. Fluorescence of zsGreen when fused with ATM is

lower than that when fused with MiniATM, which in turn is lower than that of unfused zsGreen under uniform transfection conditions. As all experiments employed 1μg of pDNA regardless of molar mass, such differences could be attributed to the correspondingly greater molar amounts of smaller plasmids as shown in Table [3]. To confirm the extent to which this molarity affects results, future transfection efficiency experiments can be assessed with the number of plasmid moles per unit number of cells kept constant. The amount of GET peptides would then need to be adapted for each plasmid, such that the charge ratio is kept constant. Fusion through the self-cleaving T2A peptide however was found to amplify the signal for plasmids carrying corresponding transgenes, suggesting that fluorescence may also be subject to noise from the fused protein. It therefore cannot be excluded that the size, function and instability of the protein fused to zsGreen could modulate interference with the signal. The relevance of these findings is to account for these factors when optimising the formulation, as they may affect the extent to which measured zsGreen fluorescence and actual transfection efficiency correlate. T2A linkage couples expression of both proteins, but rescues zsGreen from co-degradation and interaction with the unstable ATM protein. Incorporation of the reporter as a separate transgene from ATM may better reflect the transfection efficiency of the plasmid, as it precludes ATM interference altogether. This design was not employed as it decouples transcription of the two genes, and therefore precludes assessment of ATM expression. Constructs encoding zsGreen as a separate transgene or as T2A-coupled to ATM can be both employed in future experiments, to respectively assess pDNA transfection efficiency and ATM transgene expression. One limitation of T2A assays is that the extent to which ATM fusion interferes with the efficiency of self-cleavage is presently unknown. This factor may affect the extent to which fluorescence acts as a reliable measure for expression.

Another method employed in this thesis involves assessment of zsGreen fluorescence by confocal microscopy. It is associated with the aforementioned benefits and limitations common

to zsGreen fluorescence assays, which are respectively exemplified by straightforwardness of signal analysis and reliance on the surrogate measure of a reporter protein's fluorescence. Analysis via microscopy however offers some advantages over flow cytometry, as it enables localisation of the signal within the cell. An exemplar application of this feature would be assessing the efficiency of T2A cleavage. Nuclear localisation of fluorescence would reflect inefficient cleavage, such that zsGreen co-localises with ATM protein in the nucleus following cytoplasmic translation. Cytoplasmic localisation of the signal in contrast would indicate efficient cleavage, as unfused zsGreen remains in the cytoplasm post-translation. As microscopy enables the experimenter to visualise intracellular patterns of transgene expression, it would be the analytical method of choice for assessment of zsGreen fluorescence. Flow cytometry is best applied as an accompanying validation tool.

In this study, zsGreen fluorescence results for many constructs were inconsistent across flow cytometry and microscopy. Inherent differences between the two tools may have contributed to these divergences. The two assays respectively analyse suspended and adherent samples, which may affect signal detection. Flow cytometry facilitates gating of the population, enabling specific selection of the target population. Microscopy on the other hand does not support this feature. Flow cytometry is also generally more sensitive to fluorescence variations than microscopy (104), which is of relevance to the detection of signals compromised due to interference from fused ATM protein. Microscopy also requires longer duration of observation than flow cytometry, which can result in more cells undergoing fluorescence bleaching (104). These last two effects render microscopy more susceptible to false negatives. Result inconsistency however may also be attributed to shortcomings in experimental design. The same masses of pDNA and GET peptides were used to transfect 100,000 HeLa cells for flow cytometry, but 40,000 cells for microscopy. These differing relative amounts of transfection reagents per cell may have influenced results. The number of cells transfected would have to

be kept constant across both assays, on the basis of the optimal extent of confluency for transfection. The microscopy samples assayed for zsGreen fluorescence in this thesis were immunoassayed, and thus were subjected to permeabilisation by Triton X-100, blocking by glycine and BSA, and immunostaining by the primary and secondary antibodies. Any of these factors may have interfered with fluorescence. In contrast, none of the flow cytometry samples analysed for zsGreen fluorescence were immunoassayed. Future experiments comparing zsGreen fluorescence via flow cytometry and microscopy hence need to employ samples that are identically treated.

Immunocytochemistry is an additional *in vitro* technique that was employed to assess transgene expression. Results of this method can be analysed by both confocal microscopy and flow cytometry, but it is more technically challenging to conduct than zsGreen fluorescence assays. It requires permeabilisation, blocking and immunostaining steps beyond transfection, as well as identification of antibodies specific to the target protein. It however offers several advantages. The technique involves specifically detecting the target protein. It enables the localisation of protein expression within the cell, and the analysis of its intracellular concentration, stability and interactions. Antibodies can be used to immunoprecipitate the target protein for molecular functionality assays, and adapted for Western blotting (18, 24-27). Immunocytochemistry is routinely practiced in clinical pathology labs, and so can be used to confirm expression in patient-derived biopsies following gene therapy. Fluorescent proteins like zsGreen would not be incorporated in final medicinal products, as they are devoid of therapeutic relevance but can be immunogenic (62). Immunostaining can be used to demonstrate functionality, in this case by using antibodies specific to such phosphorylated substrates of the ATM kinase as p-ATM, p-p53 and γH2AX (18). Immunostaining can also be combined with other methods to analyse the extent of transgene expression, such as assessment of ATM mRNA expression by RT-PCR (18). The immunostaining protocol employed in this

study has been optimised in line with the manufacturer's instructions and the institute's standard operating procedures (105, 106). As ATM-targeting antibodies are of low specificity, ATM was tagged with a flag sequence for which a specific primary antibody is commercially available (24, 26).

Replicating zsGreen fluorescence results with immunostaining failed, and this was determined to be due to nonspecific binding of the secondary antibody. Such failure is a major limitation to the translational potential of any preclinical gene therapy project, as it precludes conclusive demonstration of expression of the target protein. This failure may be attributed to batch-related deficiencies of the antibody. Examples include undergoing an excessive number of freeze-thaw cycles, which can affect antibody structure. Using a fresh batch would solve this issue. Another possibility is that the secondary antibody may be incompatible with transfected cells due to a yet unknown mechanism, thereby staining positive in absence of the primary antibody. Alternative secondary antibodies would then need to be examined to substitute the AlexaFluor®-647 antibody. Branter et al employed the DyLight™-55 antibody, which appears to mediate specific binding in GET-transfected samples (95). Nonspecific binding may also be enabled by suboptimal immunostaining practices, which requires review of how the protocol is best conducted. Examples include inadequate BSA blocking, which is employed to inhibit nonspecific binding of the antibody to intracellular components. Another example is insufficient washing after antibody staining, which would permit persistence of unbound antibodies. It is noteworthy that this thesis has not validated the specificity of the primary antibody, which would be required for future immunostaining experiments. Even after antibody binding is optimised, inherent differences between zsGreen fluorescence and immunostaining may continue to contribute to result divergences. The latter is more susceptible to influences from ATM protein interactions, conformational changes, and degradation, as all these factors may interfere with antibody binding. T2A cleavage of zsGreen in contrast may limit the effects

of these on the reporter's fluorescence. Differences in the half-lives of zsGreen and ATM would result in dissimilar steady-state intracellular concentrations, thereby leading to variations in the measured signals.

Experimental results in this thesis suggest improvements in the transfection efficiency of ATM pDNA in HeLa cells, as assessed by flow cytometry for zsGreen fluorescence. One central objective in this thesis sought to optimise the formulation in terms of the total amount of peptide relative to that of pDNA, as measured by PDMR. Increasing the PDMR in the GET complex appears to enhance observed transfection efficiency, at least within the range examined. The optimal formulation among those tested was found to be 16.32µg FLR : 15.22µg FLH : 1.00µg pDNA per 100,000 cells, such that the PDMRs of each of FLR and FLH is doubled compared to the baseline PDMRs employed in the work of Branter et al (95). This may be explained in terms of the increased PDMR corresponding to an increase in the number of peptides interacting with each plasmid, thereby enhancing GET transfection per plasmid. Increasing the number of MDPs per plasmid may enhance overall avidity to cell membrane proteins, thereby better targeting the complex for uptake. Concurrently, increasing the number of CPPs per plasmid may bolster the interactions responsible for inducing endocytosis. One limitation of this study is that as doubling the PDMR of each peptide was found to boost transfection efficiency, higher PDMRs could have been tested to confirm the extent to which this trend can be generalised. Another as aforementioned is the lack of experimental repetitions, which prevents statistical analysis for result reproducibility. Future experiments can also examine the relationship between PDMR and physicochemical properties of the nanoparticles. Effects on stabilities and hydrodynamic diameters may provide alternative explanations on how PDMR affects transfection efficiency, and may be relevant to further development of the formulation.

These results also suggest that the synergy between FLR and FLH persists at elevated PDMRs. The mechanism behind the synergy between these two peptides is described in Section 1.5.

FLR is known to better mediate endocytic uptake by its positively charged CPP, which consists of eight arginine residues (74-76). FLH effectively mediates endosomal escape through its terminal sequence of ten histidine residues, protonation of which interferes with endosomal viability (78). This study therefore provides some evidence that while cellular uptake and endosomal escape may be considerable bottlenecks to non-viral delivery, they may be surmountable with the appropriate engineering of GET peptides. This implies that GET peptides could potentially be designed to serve specific functions, and combined at relevant PDMRs to provide multifunctional nanoparticles that overcome the individual limitations of each (74). Novel peptides may be generated by manipulating the MDP, CPP, or DNA interaction region (74). For example in the case of ATM delivery, a significant challenge is overcoming endosomal trapping to enhance transfection of the large transgene. Development of FLH by modifying the CPP of FLR may have therefore been highly relevant, as the combination of these peptides may result in a synergistic effect that addresses both endocytic uptake and endosomal escape (74, 75, 78). The non-specific delivery mediated by the FGF12 MDP of FLH and FLR was not as much of a concern, given that AT is a multisystemic disorder for which corrective transfection of various cell types may be favourable. Furthermore, as the overarching gene therapy project revolves around delivery of ATM to Purkinje cells of the cerebellum, the experimental therapy would be investigated *in vivo* via direct intracerebellar injection. This reduces the need for highly specific delivery. Targeted delivery may however be of relevance for alternative GET applications apart from AT gene therapy, such as cancer gene therapy. Such a challenge can be addressed by altering the MDP into one that interacts selectively with receptors of the target cells (74).

The requirement for elevated PDMRs to optimise transfection efficiencies carries several implications for the translational potential of GET-based gene therapy. This effect of PDMR corresponds to the transduction principle underlying CPP function, wherein high overall

positive charges mediate efficient uptake (74). Such high overall positive charges however are usually undesirable in preclinical formulations, as they can interfere with effective diffusion across such drug delivery barriers as mucus, extracellular matrices, and cerebrospinal fluid (CSF) (107, 108). Diffusion is impeded in the first two via electrostatic interactions with their negatively charged constituents, such as proteoglycans and hyaluronic acid (109). It is hampered sterically in the last by the nanoparticle complexation and aggregation with ionic constituents (107, 110). Transfection efficiencies of highly charged particles therefore tend to be compromised when assessed *in vivo* compared to when assessed *in vitro*, as suboptimal pharmacokinetic properties mask any gains in cellular uptake. The use of high PDMRs has been examined in this study, to provide a proof-of-concept for the feasibility of delivering large transgenes efficiently by GET *in vitro*. The formulation may therefore need to be further modified for translational progression as explained in Section 5.3. These employ such strategies as charge shielding by PEGylation, or neutralisation by incorporation of negatively charged polymers (75, 108, 111).

Results also suggest that MG132 may be better at stabilising ATM expression than SAHA, as assessed by flow cytometry for zsGreen fluorescence. Co-treatment with MG132 and SAHA resulted in transfection efficiencies greater than those of SAHA treatment alone, and lower than those of MG132 treatment alone. This suggests that SAHA exhibits an inhibitory effect, which interferes with expression gains achieved with MG132 treatment. Had SAHA not been associated with such residual inhibition, co-treatment with MG132 may have resulted in a synergistic effect. Caution however needs to be exercised in interpreting these results, as 24-hour treatment with MG132 can induce apoptosis and growth arrest in HeLa cells with an IC_{50} of 5μM (101). Such effects may significantly skew results, and this experiment was not repeated sufficiently to assess outcome reproducibility. Future experiments should aim to optimise the concentration and incubation period of MG132 treatment, by accounting for both

ATM expression and cell viability. Direct quantification of the effect of stabilisation regimens on ATM protein, for example in terms of half-life and steady-state intracellular concentration, was precluded by the use of the surrogate zsGreen fluorescence assay. Another limitation is that MG132 is known to inhibit the degradation of fluorescent proteins (102). The extent to which the observed enhancements in transfection efficiency reflect zsGreen stabilisation, as opposed to ATM stabilisation, is therefore unknown. Optimisation of the stabilisation regimen therefore needs to be repeated with immunostaining analysis. One reason why MG132 may be a more effective stabilising agent is that it slows down protein degradation by proteasomal inhibition, whereas SAHA induces transgene expression by histone deacetylase inhibition (66, 69). Proteasomal degradation may be a more limiting factor of ATM kinetics, and this can also be subject to further investigation via immunostaining. As mentioned in Section 1.4, SAHA treatment can stabilise or mitigate ATM expression, with the effect being cell-line dependent (103). It could be that its overall effect on ATM expression is a balance between its activator and inhibitory mechanisms, which is dependent on other factors of cellular state. This stabilising effect of SAHA may therefore be suboptimal due to residual inhibitory activity. Another explanation for suboptimal SAHA function may lie in an unfavourable interaction with GET peptides. MG132 on other hand is reported in the literature to be compatible with ATM expression and function (69). To confirm the lack of unfavourable interactions between GET peptides and MG132, transgene expression can be assessed with varying quantities of FLR and FLH under a uniform MG132 treatment regimen.

Experimentation with stabilisation regimens also carries preclinical implications. Treatment with SAHA and MG132 is of specific relevance to ATM expression, but the principle of incorporating stabilising agents in formulation development is applicable to expression analysis of unstable proteins in general. Such instabilities could arise from tight regulation, multiple interactions, large size, rapid degradation or combinations thereof (43). Stabilisation

agents have to be validated for compatibility with other transfection components. They need to lack interference with cell cycle or viability, and ideally would enhance transgene expression via a targeted mechanism. In case multiple stabilisation agents are identified, co-treatment regimens can be investigated to identify any synergistic combinations. Such agents may be tested with the intention to establish a clinical conditioning regimen, or only used for *in vitro* optimisation. In the particular case of ATM, neither SAHA nor MG132 would be translated for clinical conditioning. They both can be cytotoxic, and have non-specific interactions with numerous endogenous biomolecules (65, 68). They may thus be unsuitable for patients with genotoxic sensitivity like those of AT (37). This concern is exacerbated by the fact the GET gene therapy may require direct intracerebellar injection, rendering the localised administration of high dose cytotoxics clinically unacceptable. SAHA and MG132 have been utilised in this work solely to help visualise ATM expression *in vitro*. The functionality assays and *in vivo* experiments described respectively in Sections 5.2 and 5.3 will need to demonstrate adequate restoration of the corrected phenotype, without stabilisation regimens.

Several limitations remain that need to be addressed before establishing GET as a platform for AT gene delivery. The most significant of these is replicating the transfection efficiencies observed with zsGreen fluorescence via immunostaining. Sample sizes in the study were small, and require repetition for adequate statistical analysis. Moreover, experiments of this work have been conducted in HeLa cells, so results require validation for reproducibility in the target $ATM^{-/-}$ fibroblasts. HeLa cells were employed because their transfection profiles are amenable and reproducible, rendering them ideal for optimising formulations and transfection protocols. Target $ATM^{-/-}$ cells are more challenging to culture and transfect, such that the roughly 50% transfection efficiencies suggested in this work may not be readily translatable to them. They therefore have to be examined to account for inherent cell-specific barriers for uptake, which may require further development of the formulation. Another limitation is that although the

study provides provisional evidence for transfection of ATM pDNA, it does not examine the functionality of the translated protein. Transfection profiles can also be more comprehensively and quantitively analysed, for example by determining the number of plasmids transfected per cell and duration of transgene expression. In sum, immunostaining and functionality assays need to reproducibly demonstrate efficient transfection and functional expression in $ATM^{-/-}$ cells. Once this *in vitro* proof-of-concept concept is established, efforts can be directed toward the future directions described in Chapter 5.

Chapter 5

Conclusions & Future Directions

Conclusions & Future Directions

5.1 Conclusions:

This study aims to optimise GET formulations *in vitro* for ATM delivery in HeLa cells. Three objectives were sought. The first was to establish the positive correlation between PDMR and transfection efficiency of ATM pDNA. The second was to establish proteasomal inhibition for stabilising expression of transfected ATM. The third was to validate ATM expression using immunostaining. Provisional evidence was provided in support of the first two objectives using the zsGreen fluorescence flow cytometry assay. Experimental designs were however associated with several limitations, and experiments were not repeated sufficiently for robust statistical analysis. The third objective could not be established due to non-specific binding of the secondary antibody. Each objective had specific goals, which are outlined in Section 1.8. Below is a list of conclusions:

- The synergistic effect of incorporating both FLH and FLR in the formulation is maintained at elevated PDMRs.
- Each peptide's PDMR is a more relevant contributor to transfection efficiency than the synergy between FLH and FLR.
- Expression of ATM constructs is greatest when cells are treated with 5μM MG132, which exceeds that of co-treatment with 5μM MG132 and 10μM SAHA, which in turn exceeds that of treatment with 10μM SAHA.
- The optimal conditions for ATM expression among those tested involve transfection with mass ratios of 1.00μg pDNA : 16.32μg FLR : 15.22μg FLH.
- Larger constructs were validated to be consistently associated with lower transfection efficiencies when pDNA mass is kept constant, due to their sizes interfering directly with transfection and/or the lower number of plasmid moles per unit pDNA mass.

- T2A-linkage of zsGreen was validated to enhance the observed transfection efficiency of ATM and MiniATM, suggesting that direct fusion of zsGreen may underestimate transfection efficiency.

Factors contributing to the non-specific binding of the secondary antibody assays have not been confirmed yet. The following objectives need to be met via immunostaining, in order to conclusively validate findings of the zsGreen fluorescence flow cytometry assay:

- Validating target specificities of the primary and secondary antibodies employed.
- Establishing expression of the ATM transgene via immunostaining.
- Establishing nuclear localisation of expressed ATM proteins using microscopy.
- Establishing correspondence of the observed expression levels of the various plasmids, as assessed by confocal microscopy and flow cytometry.
- Establishing correspondence of immunostaining and zsGreen fluorescence results.

In addition to inconclusive immunostaining, this MRes study has a number of other limitations. These require addressing in future work, to provide a solid proof-of-concept for the delivery of functional ATM by GET *in vitro*. Below is a list of notable limitations:

- Low sample sizes require repetition of the experiments, to render findings more statistically robust.
- Transfection efficiencies established in HeLa cells require validation for reproducibility in target $ATM^{-/-}$ cells.
- Functionality of GET-delivered ATM requires demonstration, by providing evidence for reconstitution of the corrected phenotype in $ATM^{-/-}$ cells.

- Transfection of ATM can be further quantitatively characterised, for example by exploring the number of plasmids transfected per cell and the duration of ATM expression post-transfection in HeLa and $ATM^{-/-}$ cells.

5.2 Short-Term Future Directions:

Several short-term objectives require investigation to address the aforementioned limitations of this studies, and to establish an *in vitro* proof-of-concept for delivery of ATM pDNA via GET. These were mentioned in Chapter 4 and Section 5.1, and are reiterated here as they are essential components of short-term future directions. The first is demonstrating reproducibility of the transfection efficiencies presented in this thesis. The statistical robustness of the results can be enhanced by repeating the experiments of Chapter 3, so as to expand the sample size. The second objective is validating expression of transfected ATM by immunostaining. Results of immunostaining in Section 3.3 were inconclusive due to non-specific binding of the secondary antibody. Contribution of batch defects to non-specific binding can be validated, by examining a fresh batch of AlexaFluor®-647. Alternative antibodies can also be examined. An example is the DyLight™-55 secondary antibody (51). Immunostaining can then be applied to establish expression of ATM pDNA and nuclear localisation of ATM protein. It can also be used to validate the transfection efficiencies obtained via zsGreen fluorescence, and to confirm correspondence of microscopy and flow cytometry results. The third objective is establishing expression of transfected ATM in target $ATM^{-/-}$ cells. Both primary and immortalised $ATM^{-/-}$ cells can be examined. Transfection efficiencies can be assessed by zsGreen fluorescence and immunostaining, and analysed by microscopy and flow cytometry as described in Section 3.

Two additional short-term objectives require investigation, to establish functionality of transfected ATM in $ATM^{-/-}$ cells. The first examines such functionality at the cellular level, as described in detail in Section 5.2.1. It seeks to demonstrate reconstitution of irradiation-induced

DSB repair and of cellular responses to oxidative stress, respectively by using γ-irradiation and t-butyl hydroperoxide colony forming assays. It also seeks to demonstrate reconstitution of cell cycle abnormalities, using the G2-M arrest cell cycle assay. The second objective examines ATM functionality at the molecular level, as described in Section 5.2.2. It seeks to establish phosphorylation of ATM substrates by Western blotting and/or immunocytochemistry, following treatment of transfected $ATM^{-/-}$ cells with ATM-activating stimuli. It also seeks to establish substrate phosphorylation by immunoprecipitated ATM protein, using the *in vitro* ATM kinase assay.

5.2.1 Cellular Functionality Assays:

One important objective after optimising transfection is demonstrating functionality of the expressed protein. At the cellular level, this corresponds to restoring resistance to ionising irradiation and oxidative stress in $ATM^{-/-}$ cells (71, 72). One suitable assay to establish such functionality *in vitro* is the colony forming assay, the general structure of which is described in Section 1.4 (18, 52). Experimental designs aim to characterise the irradiation sensitivities of transfected $ATM^{-/-}$ fibroblasts, by comparing it with those of wildtype HFF-1 fibroblasts (positive control) and untransfected $ATM^{-/-}$ fibroblasts (negative control).

Experimental protocols for colony forming assays are available in the literature (18, 27, 52). $ATM^{-/-}$ fibroblasts are cultured as described in Section 2.2.1. Plating efficiency (PE) is first calculated by plating a known number of cells without irradiation treatment, and counting the number of colonies formed two weeks later (52). Colonies are taken as clusters containing more than 50 cells (52). Prior to counting, the culture is fixed with 0.5%/5.0% formaldehyde/glutaraldehyde in PBS and stained with 0.5% crystal violet (52). The equation is $PE = \frac{Number\ of\ Colonies\ Formed}{Number\ of\ Cell\ Seeded}$ (52).The surviving fraction (SF) is calculated by repeating

the experiment as for PE, but with irradiation at the desired dose immediately after plating (52). The equation used is $SF = \frac{Number\ of\ Colonies\ Formed\ After\ Treatment}{Number\ of\ Cells\ Seeded \times PE}$ (52). To fully characterise sensitivities, increasing irradiation doses can be employed (52). Graphs of SF vs irradiation dose can be generated to compare sensitivities of transfected ATM$^{-/-}$ cells with those of positive and negative controls. A variation of this assay inspects cellular sensitivity to oxidative stress, by substituting irradiation with exposure to 10mM t-butyl hydroperoxide for 15 minutes (27).

Another cellular functionality assay examines the extent to which ATM transfection modifies cell cycle abnormalities (18, 24). Controls are as for the previous assay. ATM$^{-/-}$ cells are transfected, and treated either with irradiation or t-butyl hydroperoxide as described above (18, 24). They are fixed in 70% ethanol and incubated in DNA extraction buffer. Extracts are resuspended in a PBS solution of RNase and propidium iodide, and incubated in the dark (112). Propidium iodide stains both DNA and RNA, so RNase is added as only DNA is relevant to cell cycle analysis (112). DAPI selectively stains DNA and can substitute propidium iodide , in which case RNase is not needed (112). The samples are analysed by flow cytometry (112). Two peaks are obtained, with the one further shifted corresponding to cells in the G2/M phase (112). The other corresponds to cells in the G0/G1 phase (112). ATM$^{-/-}$ cells are arrested at the G2-M phase post irradiation, so functionality is demonstrated if the ratio $\frac{Number\ of\ Cells\ in\ G_2-M\ Phase}{Number\ of\ Cells\ in\ G_0-1\ Phase}$ is reduced in transfected cells compared to the negative controls (18, 24).

5.2.2 Molecular Functionality Assays:

Western blotting is a commonly used assay to demonstrate ATM functionality at the molecular level, namely by immunostaining substrates of ATM kinase in their phosphorylated states (18, 24-27). Transfected ATM$^{-/-}$ cells and controls are treated with irradiation or oxidative stress as

for the clonogenic assays of Section 5.2.1 (18, 24-27). Nuclear lysates are extracted using commercial kits, run on electrophoresis gels, blocked for 1h, and incubated with the relevant primary antibodies overnight (18). Samples are then stained with the fluorophore-conjugated secondary antibody (18). Primary antibodies can target p-ATM, γH2AX, and p-p53, among others (18). Alternatively, immunocytochemistry assays can be employed as described in Section 1.4, wherein the primary antibodies used would target the phosphorylated ATM substrates. Untransfected $ATM^{-/-}$ cells in both Western blotting and immunocytochemistry would stain negative, as phosphorylation depends on activation of functional ATM in response to stress (18). To demonstrate functional reconstitution, transfected $ATM^{-/-}$ cells should stain positive in a manner comparable to wildtype fibroblasts (18).

Another assay to demonstrate molecular functionality of transfected ATM is the *in vitro* kinase assay (24). $ATM^{-/-}$ cells are transfected with flag-tagged ATM (24). Cell extracts are then prepared using a lysis buffer, and immunoprecipitated with immobilised anti-flag primary antibody (24). The immunoprecipitant is then resuspended for 30 minutes in kinase buffer, which contains radiolabelled [γ^{32}P]-ATP and the substrate p53 (24). The reaction is stopped with SDS-polyacrylamide buffer, which also enables running the sample on an electrophoresis gel (24). The p53 band is inspected for radioactivity (24). As p53 is a direct substrate of ATM kinase activity, the result would be positive solely with functional ATM.

5.3 Long-Term Directions:

Long-term goals seek to provide evidence for the translational potential of the experimental therapy, by characterising the projected pharmacokinetics and pharmacodynamics of ATM/GET nanoparticles. They would build on the evidence for *in vitro* transfection of functional ATM from Section 5.2, by accounting for delivery barriers that may affect i*n vivo*

delivery, expression and functionality. The long-term plan therefore seeks to explore the following objectives:

- Optimising nanoparticle design *in vitro* for effective biodistribution and gene delivery to the brain, as discussed in Section 5.3.1
- Optimising the formulation for sustainable ATM expression by combining GET delivery with genomic integration, as discussed in Section 5.3.2
- Characterising the pharmacokinetics and pharmacodynamics of the nanoparticles *in vivo* using relevant animal models, as discussed in Section 5.3.3
- Exploration of alternative modalities for GET-based delivery of ATM, as discussed in Section 5.3.4.

5.3.1 Optimisation of GET for Brain Delivery:

Several strategies can be applied to optimise GET particles for uptake in the central nervous system. The main target in AT is Purkinje cells, for which several barriers to drug delivery exist. One aspect of the current design that may interfere with GET efficacy is the high charge ratio used. Positively charged nanoparticles have suboptimal bio-diffusion properties, as they are unable to efficiently cross biological barriers (76, 107-109). They are readily entrapped via electrostatic interactions in biological media such as mucus and extracurricular matrices (75, 109). This is because these barriers contain highly negative charged constituents, such as mucins, proteoglycans and hyaluronic acid (75, 109). Nanoparticles also form complexes and aggregates within physiological ionic environments, which exacerbates steric interferences with diffusion in such media as the CSF (75, 107, 110).

One approach to enhance the efficacy of such delivery is the controlled PEGylation of GET peptides (75). As discussed in Section 1.6, this has been applied to optimise pulmonary

transfection *in vivo* (75). PEGylation enhances diffusion properties of GET particles in biological fluids, by shielding the positive charges of CPPs (75). It also improves the stability of their cargoes against enzymatic degradation (75). The relative content of PEGylated peptides to their unPEGylated counterparts has to be optimised (75). This is because charge shielding interferes with CPP-mediated GET delivery, so an appropriate balance between bio-diffusion properties and transfection efficiency has to be achieved (75). For pulmonary delivery for instance, a PEGylation rates of 40% was found to be optimal (75). An alternative approach involves overall neutralisation of the nanoparticle charge, by incorporation of negatively charged polymers in the formulation (75, 108, 111). These would enhance diffusion and stability in biological barriers, as has been described in the literature for gastrointestinal mucus (75, 108, 111). They however may interfere with the efficiency of GET uptake as PEG does (75, 108, 111). Their content in the formulation therefore has to be optimised relative to GET peptides (75, 108, 111). Several assays are available for *in vitro* projection of brain delivery, such as particle tracking analysis (113). GET/ATM nanoparticles can also be investigated for distribution and transfection in neuronal cultures, wherein they would be analysed by immunostaining or reporter fluorescence as described in Section 1.4 (108).

5.3.2 Optimisation of Sustainable Expression of ATM:

Genomic integration could mediate sustainable expression of ATM following GET delivery (108). As discussed in Section 1.6, various methods can be applied. Transposition requires flanking the transgene with transposon sequences, and codelivery of transposases as GET-tagged proteins or as mRNA complexed with GET peptides (90, 91, 108). Integration via Cas9 or dCas9-Hsmar1 requires co-transduction of GET-tagged ribonucleoproteins, or co-transfection of their mRNA and gRNA as GET complexes (89-94). Transposases and Cas9 are

not delivered as pDNA, as their overexpression can be genotoxic (94). The gRNA is ideally targeted to the endogenous or AAVS1 sites (26, 108).

Several assays can be employed to characterise transgene sustainability. The first aim is to demonstrate genomic insertion. This would be achieved by extracting genomic DNA from transfected cells, and running PCR using primers specific to transfected DNA (18, 26, 108). The second aim is to establish sustained expression and functionality of the transgene (18, 25, 26, 108). This can be analysed at the protein level by zsGreen fluorescence or immunostaining at different time points, using microscopy or flow cytometry as described in this thesis. Alternatively, ATM mRNA levels can be assessed at different time points by RT-PCR (18, 108). Such assays can be tested *in vitro* in HeLa cells, neuronal cultures and $ATM^{-/-}$ fibroblasts (108). They also can be examined *in vivo* using murine models as explained below (25, 26). Effects of single and repeat administrations can also be investigated, as the latter may result in accumulation of transgenic integration over time (108).

5.3.3 *In Vivo* Experimentation with GET/ATM Nanoparticles:

The first set of *in vivo* experiments would aim at establishing the pharmacokinetic properties of GET/ATM nanoparticles. Pharmacokinetic assays can be conducted in healthy mice, wherein fluorophore-labelled nanoparticles can be tracked for distribution and elimination profiling (114). One anticipated challenge with the translational potential of this project pertains to the route of administration, as the ataxic hallmark of AT is thought to originate from the Purkinje cells of the cerebellum. Nanoparticles may be unable to cross the blood-brain barrier following intravenous (IV) administration. Various routes of administration for central delivery can therefore be examined, including direct cerebellar injection (27, 114). Less invasive routes can also be examined, such as the intranasal, intrathecal and intra-orbital routes (114). To characterise the biodistribution of the nanoparticles, sections corresponding to the

various regions of the brain, delivery tracts and relevant organs can be analysed for fluorescence (114-116). The half-life of the nanoparticles can be determined by inspecting fluorescence at various time points. The optimal dosing regimen would be established, by examining fluorescence following single and serial dose administrations (114).

Pharmacodynamic assays aim to establish the safety and efficacy of this experimental therapy. Efficacy assays would initially assess transfection efficiencies of plasmids encoding fluorescent or bioluminescent proteins in healthy mice. Whole animals would be imaged live, and assessed for expression using bioluminescence quantification assays at different time points (114-116). Relevant organs can be harvested and examined with microscopy, with an emphasis on brain sections and delivery tracts (114-116). AT is a multi-systemic disorder, so IV administration can be analysed for correction of AT manifestations in relevant peripheral organs. Once *in vivo* transfection is established, the therapy can be assessed for efficacy of ATM delivery in murine AT models. Expression of ATM would be examined at the mRNA level using RT-PCR, and at the protein level using immunostaining (18). Assessments can look into such AT associations as neurodegeneration rate, longevity, sensitivity to irradiation, and susceptibility to cancer (45-47). The safety profile can be examined, by analysing brain sections and the CSF for such inflammatory biomarkers as cytokines (86, 114).

5.3.4 Alternative GET Approaches for AT Therapy:

This thesis mainly investigates pDNA delivery of ATM, which corresponds to the first modality described in Section 1.6. Such preparations are stable, cheap, simple, and easy to reconstitute (75). They demonstrate reproducible transfections, and can be freeze-dried for storage (75, 108). Excipient minimalism is also of relevance to the intra-cerebral administration of ATM plasmids, as it reduces the toxicity risk of such an invasive procedure. Other delivery options however can be investigated, such as the third modality that corresponds to

recombinant protein delivery (83). The rationale is that such recombinant proteins may have more suitable biodistribution, transduction or functionality profiles *in vivo*. As has been established with RUNX2 and MyoD delivery, recombinant ATM protein would be tagged on the N-terminus with a CPP and an MDP (83, 84). Amphiphilic domains like LK15 would not be needed, as they have been incorporated in FLR and FLH to bind nucleic acids (74). ATM structure incorporates such eukaryotic PTMs as disulphide bridges on residue C2991, and requires TTT as a cochaperone for protein folding (10, 11). It therefore is best expressed in mammalian cells, followed by isolation via immunoprecipitation (79). It can be modified as described in this thesis for immunostaining and zsGreen fluorescence assays, so as to establish *in vitro* uptake. It can also be examined using the cellular and molecular functionality assays described in Sections 5.2.1. and 5.2.2. Fluorophore-tagged versions can determine its pharmacokinetics *in vivo* (79), whereas administration to murine AT models can establish its preclinical efficacy. The protein can be examined for immunogenicity, as it will require repeat administration (79).

Delivery of ATM can be augmented by the second modality, which corresponds to the combination of GET delivery with microparticle encapsulation. Such a formulation would enable controlled release from an implant, thereby reducing the need for repeat administration (82). It would be particularly relevant if *in vivo* experimentation reveals that efficacy of the first modality requires repeat administration of GET/ATM nanoparticles via direct cerebellar injection. The second modality would also protect the therapeutic agent from extracellular enzymatic degradation, thereby prolonging its half-life (82). In one embodiment, ATM pDNA would be complexed with GET peptide, and the complexes encapsulated in PLGA/PEG microparticles. In another embodiment, recombinant GET-tagged recombinant ATM protein would be encapsulated in PLGA/PEG microparticles (79, 85). These formulations can be examined for *in vitro* and *in vivo* performances using the various assays described in this thesis.

EryDex® proposes the therapeutic utility of MiniATM, which encodes a fragment of the ATM protein to partially reconstitute the AT phenotype (32-34). This warrants the investigation of alternatively-spliced versions of ATM for efficacy. Given the observed negative correlation between transfection efficiency and construct size, such agents may enable a satisfactory compromise between transfection efficiency and protein functionality. Synthetic variants can be systemically generated by truncating domains of ATM (79). Such agents may be delivered as pDNA or recombinant proteins, and characterised using the various delivery and functionality assays described in this thesis.

5.4 Clinical Outlook of GET-Mediated AT Gene Therapy:

Given the complexity of the suggested future directions, it is relevant to elaborate on the outlook for the clinical translation of GET-mediated ATM delivery. One strength of the proposed therapy would be its delivery of the full-length transgene, thereby potentially providing a universal treatment for all AT patients. This is of particular relevance given that AT is an ultra-rare condition with a multitude of identified causative mutations (43). Full-length gene delivery would bypass the need to manufacture personalised formulations, thereby reducing the costs of development, commercialisation and clinical adoption. AT is a multisystemic disorder, so effective treatment would require delivering the GET nanoparticles to various implicated organs. Section 5.3.1 exemplifies how the formulation can be developed for brain delivery, as neurological manifestations are major sources of AT morbidity (4). Immunodeficiencies, cancers, and pulmonary deterioration are however major contributors to mortality (4). Pulmonary GET delivery as reported in the literature may therefore be needed to deliver functional ATM to the lung, whereas systemic IV administration may be suitable for immunological and haematological reconstitution (4, 75). GET therapy for the latter targets may alternatively be implemented via reduced-conditioning autologous BMT, such that

patient-derived HSCs are transfected *ex vivo* and re-engrafted in a manner similar to LV therapy in primary immunodeficiencies (19, 20, 37). Treatment of each manifestation may be inspected in a dedicated clinical trial, such that clinical translation for each intendent organ is kept independent. GET peptides have a satisfactory safety profile, as they are known to be of little immunogenicity (75). This permits repeat administration to each implicated organ, so as to enable accumulation of the transgene and boost efficacy. It also permits multiple administration to various organs, so as to provide a comprehensive treatment for the multiple manifestations of AT. Such clinical translation may result in a truly disease-modifying therapy, thereby shifting the paradigm for AT treatment.

GET-mediated delivery of ATM pDNA is projected to compare favourably to the AT experimental therapies described in Section 1.3. According to zsGreen-fluorescence cytometry, transfection efficiencies up to 50% of ATM pDNA may be permissible with GET delivery in HeLa cells. This figure is projected to be high enough to attempt genomic integration strategies through Cas9, and to experiment with delivery *in vivo*. It is difficult to compare this figure with the transfection efficiencies of the viral vectors, as these have been examined with different cell lines and treatment procedures. For example, the transfection efficiency of LVs was found to be around 20% in otherwise untreated $ATM^{-/-}$ cells (18). GET peptides however are free from the biohazards associated with viral vectors (15). LVs for example are associated with insertional mutagenesis, contain undesirable regulatory proteins, and carry the risk of recombining to form replication-competent viroids (15). HSV-amplicon vectors are associated with residual cytotoxicity and recombination with latent HSV, whereas adenoviral vectors are highly immunogenic (15). Pre-existing immunity in the general population may preclude the use of the last two vectors (15). Even in patients without pre-existing immunity, immunogenicity precludes serial dosing (15). GET delivery does not require high-intensity conditioning as seen with allogenic BMT, to which AT patients are particularly sensitive (37).

Delivering the full-length ATM gene is highly likely to better reconstitute normal function than the truncated MiniATM of Erydex®, which is devoid of several key regulatory and functional domains (32). Full-length gene delivery also offers a universal treatment for AT patients, as opposed to the mutation-specific genome editing approach (43).

The future directions described in this Chapter may provide further basis for the utility of GET as a general platform technology for gene delivery, beyond AT gene therapy. GET is projected to have transfection efficiencies significantly lower than those of LVs and AAVs, and so is particularly appropriate for transgenes incompatible with viral delivery. This is exemplified by transgenes that exceed the packaging capacity of viral vectors, as is the case with ATM. Other examples of such large genes include DMD, ATR, and TTN, mutations in which can respectively manifest as Duchenne muscular dystrophy, Seckel syndrome, and various hereditary myopathies (21, 117, 118). GET delivery is also a highly relevant technology for repeat-administration gene delivery protocols, as they are of low immunogenicity and compatible biodegradability (75). They therefore can be purposed for such protocols, wherein the applicability of several viral vectors is limited due to immunogenicity.

References

References

1. Amirifar P, Ranjouri MR, Yazdani R, Abolhassani H, Aghamohammadi A. Ataxia-telangiectasia: A review of clinical features and molecular pathology. Pediatric allergy and immunology. 2019;30(3):277-88.

2. McKinnon P. ATM and ataxia telangiectasia. EMBO Reports. 2004;5(8):772-6.

3. McKinnon PJ. ATM and the Molecular Pathogenesis of Ataxia Telangiectasia. Annual review of pathology. 2012;7(1):303-21.

4. Rothblum-Oviatt C, Wright J, Lefton-Greif MA, McGrath-Morrow SA, Crawford TO, Lederman HM. Ataxia telangiectasia: a review. Orphanet journal of rare diseases. 2016;11(1):159-21.

5. Rotman G. ATM: from gene to function. Human molecular genetics. 1998;7(10):1555-63.

6. Amirifar P, Ranjouri M, Lavin M, Abolhassani H, Yazdani R, Aghamohammadi A. Ataxia-telangiectasia: epidemiology, pathogenesis, clinical phenotype, diagnosis, prognosis and management. Expert Review of Clinical Immunology. 2020;16(9):859-71.

7. Khanna KK, Lavin MF, Jackson SP, Mulhern TD. ATM, a central controller of cellular responses to DNA damage. Cell death and differentiation. 2001;8(11):1052-65.

8. Takao N, Li Y, Yamamoto K-i. Protective roles for ATM in cellular response to oxidative stress. FEBS Letters. 2000;472(1):133-6.

9. Turenne GA, Paul P, Laflair L, Price BD. Activation of p53 transcriptional activity requires ATM's kinase domain and multiple N-terminal serine residues of p53. Oncogene. 2001;20(37):5100-10.

10. Shiloh Y, Ziv Y. The ATM protein kinase: regulating the cellular response to genotoxic stress, and more. Nature reviews Molecular cell biology. 2013;14(4):197-210.

11. Maréchal A, Zou L. DNA Damage Sensing by the ATM and ATR Kinases. Cold Spring Harbor Perspectives in Biology. 2013;5(9): a012716.

12. Ziv Y, Bar-Shira A, Pecker I, Russell P, Jorgensen TJ, Tsarfati I, et al. Recombinant ATM protein complements the cellular A-T phenotype. Oncogene. 1997;15(2):159-67.

13. Ning Z, Philip C, Khanna, Shaun S, Magtouf G, Sergei K, et al. Isolation of Full-Length ATM cDNA and Correction of the Ataxia-Telangiectasia Cellular Phenotype. Proceedings of the National Academy of Sciences - PNAS. 1997;94(15):8021-6.

14. Mülhardt CB, EW. Investigating the Function of DNA Sequences. In: Cornel Mülhardt EWB, editor. Molecular Biology and Genomics: Academic Press; 2007. p. 169-221.

15. Vannucci L, Lai M, Chiuppesi F, Ceccherini-Nelli L, Pistello M. Viral vectors: A look back and ahead on gene transfer technology. The new microbiologica. 2013;36:1-22.

16. Ingusci S, Verlengia G, Soukupova M, Zucchini S, Simonato M. Gene Therapy Tools for Brain Diseases. Frontiers in pharmacology. 2019;10:724.

17. Nathwani AC, Gray JT, Ng CYC, Zhou J, Spence Y, Waddington SN, et al. Self-complementary adeno-associated virus vectors containing a novel liver-specific human factor IX expression cassette enable highly efficient transduction of murine and nonhuman primate liver. Blood. 2006;107(7):2653-61.

18. Carranza D, Torres-Rusillo S, Ceballos-Pérez G, Blanco-Jimenez E, Muñoz-López M, García-Pérez JL, et al. Reconstitution of the Ataxia-Telangiectasia Cellular Phenotype With Lentiviral Vectors. Frontiers in immunology. 2018;9:2703.

19. Aiuti A, Biasco L, Scaramuzza S, Ferrua F, Cicalese MP, Baricordi C, et al. Lentivirus-based Gene Therapy of Hematopoietic Stem Cells in Wiskott-Aldrich Syndrome. Science (New York, NY). 2013;341(6148):1233151-.

20. Biffi A, Montini E, Lorioli L, Cesani M, Fumagalli F, Plati T, et al. Lentiviral Hematopoietic Stem Cell Gene Therapy Benefits Metachromatic Leukodystrophy. Science (American Association for the Advancement of Science). 2013;341(6148):1233158-.

21. Counsell JR, Asgarian Z, Meng J, Ferrer V, Vink CA, Howe SJ, et al. Lentiviral vectors can be used for full-length dystrophin gene therapy. Scientific reports. 2017;7(1):44775.

22. Merten O-W, Hebben M, Bovolenta C. Production of lentiviral vectors. Molecular therapy Methods & clinical development. 2016;3(C):16017.

23. 770. In Vitro and In Vivo ATM Gene Expression Mediated by HSV Amplicon Vector. Molecular therapy. 2002;5(5):S252-S.

24. Cortés ML, Bakkenist CJ, Di Maria MV, Kastan MB, Breakefield XO. HSV-1 amplicon vector-mediated expression of ATM cDNA and correction of the ataxia-telangiectasia cellular phenotype. Gene therapy. 2003;10(16):1321-7.
25. Cortés ML, Oehmig A, Perry KF, Sanford JD, Breakefield XO. Expression of human ATM cDNA in Atm-deficient mouse brain mediated by HSV-1 amplicon vector. Neuroscience. 2006;141(3):1247-56.
26. Cortés ML, Oehmig A, Saydam O, Sanford JD, Perry KF, Fraefel C, et al. Targeted Integration of Functional Human ATM cDNA Into Genome Mediated by HSV/AAV Hybrid Amplicon Vector. Molecular therapy. 2008;16(1):81-8.
27. Qi J, Shackelford R, Manuszak R, Cheng D, Smith M, Link CJ, et al. Functional expression of ATM gene carried by HSV amplicon vector in vitro and in vivo. Gene therapy. 2004;11(1):25-33.
28. Ryan M, Rodney S, Charles JL, Suming W. 538. Functional Correction of A-T Cells by ATM Gene Expression Mediated by HSV Amplicon Vector after the Ionizing Radiation or under Oxidative Stress Condition. Molecular therapy. 2004;9(S1):S203-S.
29. RJ C, MS S, CP V. Recombinant adeno-associated viral integration and genotoxicity: insights from animal models. Human Gene Therapy. 2017;28(4):314-22.
30. F L, H K, M V, A B. Biosafety of gene therapy vectors derived from herpes simplex virus type 1. Current Gene Therapy. 2013;13(6):478-91.
31. Chessa L, Leuzzi V, Plebani A, Soresina A, Micheli R, D'Agnano D, et al. Intra-Erythrocyte Infusion of Dexamethasone Reduces Neurological Symptoms in Ataxia Teleangiectasia Patients: Results of a Phase 2 Trial. Orphanet journal of rare diseases. 2014;9(1):5-.
32. Menotta M, Biagiotti S, Bianchi M, Chessa L, Magnani M. Dexamethasone partially rescues ataxia telangiectasia-mutated (ATM) deficiency in ataxia telangiectasia by promoting a shortened protein variant retaining kinase activity. The Journal of biological chemistry. 2012;287(49):41352-63.
33. Menotta M, Biagiotti S, Spapperi C, Orazi S, Rossi L, Chessa L, et al. ATM splicing variants as biomarkers for low dose dexamethasone treatment of A-T. Orphanet journal of rare diseases. 2017;12(1):126-7.
34. Menotta M, Orazi S, Gioacchini AM, Spapperi C, Ricci A, Chessa L, et al. Proteomics and transcriptomics analyses of ataxia telangiectasia cells treated with Dexamethasone. PloS one. 2018;13(4):e0195388-e.
35. Biagiotti S, Menotta M, Orazi S, Spapperi C, Brundu S, Fraternale A, et al. Dexamethasone improves redox state in ataxia telangiectasia cells by promoting an NRF2-mediated antioxidant response. The FEBS journal. 2016;283(21):3962-78.
36. Biagiotti S, Bianchi M, Rossi L, Chessa L, Magnani M. Activation of NRF2 by dexamethasone in ataxia telangiectasia cells involves KEAP1 inhibition but not the inhibition of p38. PloS one. 2019;14(5):e0216668-e.
37. Slack J, Albert MH, Balashov D, Belohradsky BH, Bertaina A, Bleesing J, et al. Outcome of hematopoietic cell transplantation for DNA double-strand break repair disorders. Journal of allergy and clinical immunology. 2018;141(1):322-8.e10.
38. Duecker R, Baer PC, Buecker A, Huenecke S, Pfeffermann L-M, Modlich U, et al. Hematopoietic Stem Cell Transplantation Restores Naïve T-Cell Populations in Atm-Deficient Mice and in Preemptively Treated Patients With Ataxia-Telangiectasia. Frontiers in immunology. 2019;10:2785-.
39. Pietzner J, Baer PC, Duecker RP, Merscher MB, Satzger-Prodinger C, Bechmann I, et al. Bone marrow transplantation improves the outcome of A*tm* -deficient mice through the migration of ATM-competent cells. Human Molecular Genetics. 2013;22(3):493-507.
40. Bagley J, Cortes ML, Breakefield XO, Iacomini J. Bone marrow transplantation restores immune system function and prevents lymphoma in Atm-deficient mice. Blood. 2004;104(2):572-8.
41. Bakhtiar S, Woelke S, Huenecke S, Kieslich M, Taylor AM, Schubert R, et al. Pre-emptive Allogeneic Hematopoietic Stem Cell Transplantation in Ataxia Telangiectasia. Frontiers in immunology. 2018;9:2495-.
42. Beier R, Sykora KW, Woessmann W, Maecker-Kolhoff B, Sauer M, Kreipe HH, et al. Allogeneic-matched sibling stem cell transplantation in a 13-year-old boy with ataxia telangiectasia and EBV-positive non-Hodgkin lymphoma. Bone marrow transplantation (Basingstoke). 2016;51(9):1271-4.

43. Prakash V. Gene Editing in Prkdc Severe Combined Immunodeficiency and Ataxia Telangiectasia: Royal Holloway University of London; 2017 (Thesis).
44. Barlow C, Hirotsune S, Paylor R, Liyanage M, Eckhaus M, Collins F, et al. Atm-Deficient Mice: A Paradigm of Ataxia Telangiectasia. Cell (Cambridge). 1996;86(1):159-71.
45. Xu Y, Ashley T, Brainerd EE, Bronson RT, Meyn MS, Baltimore D. Targeted disruption of ATM leads to growth retardation, chromosomal fragmentation during meiosis, immune defects, and thymic lymphoma. Genes & development. 1996;10(19):2411-22.
46. Di Siena S, Campolo F, Gimmelli R, Di Pietro C, Marazziti D, Dolci S, et al. Atm reactivation reverses ataxia telangiectasia phenotypes in vivo. Cell death & disease. 2018;9(3):314-13.
47. Perez H, Abdallah M, Chavira J, Egeland M, Vo K, Profile VOVO, et al. A novel, ataxic mouse model of Ataxia Telangiectasia caused by a clinically relevant nonsense mutation. BioRxiv. 2020 (Preprint; Not Formally Peer-Reviewed).
48. Yates JL, Warren N, Sugden B. Stable replication of plasmids derived from Epstein–Barr virus in various mammalian cells. Nature (London). 1985;313(6005):812-5.
49. Autofluorescence; https://www.bio-rad-antibodies.com/flow-cytometry-autofluorescence.html; bio-rad.
50. Goat Anti-Mouse IgG H&L (Alexa Fluor® 647); https://www.abcam.com/goat-mouse-igg-hl-alexa-fluor-647-ab150115.html?productWallTab=ShowAll2020; Abcam.
51. DyLight Fluors Technology and Product Guide; https://www.thermofisher.com/uk/en/home/life-science/protein-biology/protein-labeling-crosslinking/protein-labeling/fluorescent-protein-labeling/dylight-fluors-technology-product-guide.html; Thermo Fisher Scientific.
52. Franken NAP, Rodermond HM, Stap J, Haveman J, van Bree C. Clonogenic assay of cells in vitro. Nature protocols. 2006;1(5):2315-9.
53. Balmus G, Pilger D, Coates J, Demir M, Sczaniecka-Clift M, Barros AC, et al. ATM orchestrates the DNA-damage response to counter toxic non-homologous end-joining at broken replication forks. Nature communications. 2019;10(1):87-.
54. Köcher S, Spies-Naumann A, Kriegs M, Dahm-Daphi J, Dornreiter I. ATM is required for the repair of Topotecan-induced replication-associated double-strand breaks. Radiotherapy and oncology. 2013;108(3):409-14.
55. Tanaka T, Huang X, Halicka HD, Zhao H, Traganos F, Albino AP, et al. Cytometry of ATM activation and histone H2AX phosphorylation to estimate extent of DNA damage induced by exogenous agents. Cytometry Part A. 2007;71A(9):648-61.
56. Fu X, Wan S, Lyu YL, Liu LF, Qi H. Etoposide Induces ATM-Dependent Mitochondrial Biogenesis through AMPK Activation. PloS one. 2008;3(4):e2009-e.
57. Korwek Z, Sewastianik T, Bielak-Zmijewska A, Mosieniak G, Alster O, Moreno-Villaneuva M, et al. Inhibition of ATM blocks the etoposide-induced DNA damage response and apoptosis of resting human T cells. DNA repair. 2012;11(11):864-73.
58. Tanaka T, Dorota Halicka H, Traganos F, Seiter K, Darzynkiewicz Z. Induction of ATM activation, histone H2AX phosphorylation and apoptosis by etoposide: relation to cell cycle phase. Cell Cycle. 2007;6(3):371-6.
59. Álvarez-Quilón A, Serrano-Benítez A, Ariel Lieberman J, Quintero C, Sánchez-Gutiérrez D, Escudero LM, et al. ATM specifically mediates repair of double-strand breaks with blocked DNA ends. Nature communications. 2014;5(1):3347-.
60. Matz MV, Fradkov AF, Labas YA, Savitsky AP, Zaraisky AG, Markelov ML, et al. Fluorescent proteins from nonbioluminescent Anthozoa species. Nature biotechnology. 1999;17(10):969-73.
61. zsGreen; https://www.fpbase.org/protein/zsgreen/; Fluorescent Protein Database; 2021.
62. Bell P, Vandenberghe LH, Wu D, Johnston J, Limberis M, Wilson JM. A Comparative Analysis of Novel Fluorescent Proteins as Reporters for Gene Transfer Studies. The journal of histochemistry and cytochemistry. 2007;55(9):931-9.
63. Kim JH, Lee S-R, Li L-H, Park H-J, Park J-H, Lee KY, et al. High Cleavage Efficiency of a 2A Peptide Derived from Porcine Teschovirus-1 in Human Cell Lines, Zebrafish and Mice. PloS one. 2011;6(4):e18556.

64. Szymczak AL, Workman CJ, Wang Y, Vignali KM, Dilioglou S, Vanin EF, et al. Correction of multi-gene deficiency in vivo using a single 'self-cleaving' 2A peptide–based retroviral vector. Nature biotechnology. 2004;22(5):589-94.
65. Richon VM. Cancer biology: mechanism of antitumour action of vorinostat (suberoylanilide hydroxamic acid), a novel histone deacetylase inhibitor. British journal of cancer. 2006;95(S1):S2-S6.
66. Singh S, Le H, Shih S-J, Ho B, Vaughan AT. SAHA modification of chromatin architecture affects DNA break formation and repair. International journal of radiation oncology, biology, physics. 2010;76(2):566.
67. Thurn KT, Thomas S, Raha P, Qureshi I, Munster PN. Histone Deacetylase Regulation of ATM-Mediated DNA Damage Signaling. Molecular cancer therapeutics. 2013;12(10):2078-87.
68. Marzano V, Santini S, Rossi C, Zucchelli M, apos, Alessandro A, et al. Proteomic profiling of ATM kinase proficient and deficient cell lines upon blockage of proteasome activity. Journal of Proteomics. 2012;75(15):4632-46.
69. Smith RJ, Savoian MS, Weber LE, Park JH. Ataxia telangiectasia mutated (ATM) interacts with p400 ATPase for an efficient DNA damage response. BMC molecular biology. 2016;17(1):22.
70. Zhou Yea. Regulation of the DNA Damage Response by DNAPKcs Inhibitory Phosphorylation of ATM. Molecular Cell. 2017;65(1):91-104.
71. Momčilović O, Choi S, Varum S, Bakkenist C, Schatten G, Navara C. Ionizing radiation induces ATM dependent checkpoint signaling and G2 but not G1 cell cycle arrest in pluripotent human embryonic stem cells. Stem Cells (Dayton, Ohio). 2009;27(8):1822-35.
72. Pandita TK, Lieberman HB, Lim DS, Dhar S, Zheng W, Taya Y, et al. Ionizing radiation activates the ATM kinase throughout the cell cycle. Oncogene. 2000;19(11):1386-91.
73. Ariumi Y, Turelli P, Masutani M, Trono D. DNA Damage Sensors ATM, ATR, DNA-PKcs, and PARP-1 Are Dispensable for Human Immunodeficiency Virus Type 1 Integration. Journal of virology. 2005;79(5):2973-8.
74. Dixon JE, Osman G, Morris GE, Markides H, Rotherham M, Bayoussef Z, et al. Highly efficient delivery of functional cargoes by the synergistic effect of GAG binding motifs and cell-penetrating peptides. Proceedings of the National Academy of Sciences - PNAS. 2016;113(3):E291-E299..
75. Osman G, Rodriguez J, Chan SY, Chisholm J, Duncan G, Kim N, et al. PEGylated enhanced cell penetrating peptide nanoparticles for lung gene therapy. Journal of controlled release. 2018;285:35-45.
76. Abu-Awwad HA-DM, Thiagarajan L, Dixon JE. Controlled release of G AG-binding enhanced transduction (GET) peptides for sustained and highly efficient intracellular delivery. Acta biomaterialia. 2017;57:225-37.
77. Ferreras L, Scott D, Reina S, Roach P, Torres T, Goya G, et al. Enhanced Cellular Transduction of Nanoparticles Resistant to Rapidly Forming Plasma Protein Coronas. Advanced Biosystems. 2020;4(10).

78. Midoux P, Pichon C, Yaouanc J-J, Jaffrès P-A. Chemical vectors for gene delivery: a current review on polymers, peptides and lipids containing histidine or imidazole as nucleic acids carriers. British Journal of Pharmacology. 2009;157(2):166-78.
79. Dixon J, Ferreras L. Recombinant ATM kinase therapy for ataxia telangiectasia (A-T). University of Nottingham: AT Children's Project; 2018 (Grant Application).
80. Alton EWFW, Armstrong DK, Ashby D, Bayfield KJ, Bilton D, Bloomfield EV, et al. A randomised, double-blind, placebo-controlled trial of repeated nebulisation of non-viral cystic fibrosis transmembrane conductance regulator (CFTR) gene therapy in patients with cystic fibrosis. Efficacy and mechanism evaluation. 2016;3(5):1-210.
81. Griesenbach U, Alton EWFW. Gene transfer to the lung: Lessons learned from more than 2 decades of CF gene therapy. Advanced drug delivery reviews. 2009;61(2):128-39.
82. Jalal AR, Dixon JE. Efficient Delivery of Transducing Polymer Nanoparticles for Gene-Mediated Induction of Osteogenesis for Bone Regeneration. Frontiers in bioengineering and biotechnology. 2020;8:849-.
83. Thiagarajan L, Abu-Awwad HA-DM, Dixon JE. Osteogenic Programming of Human Mesenchymal Stem Cells with Highly Efficient Intracellular Delivery of RUNX2. Stem cells translational medicine. 2017;6(12):2146-59.

84. Eltaher HM, Yang J, Shakesheff KM, Dixon JE. Highly efficient intracellular transduction in three-dimensional gradients for programming cell fate. Acta Biomaterialia. 2016;41:181-92.
85. Abu Awwad HA-DM, Thiagarajan L, Kanczler JM, Amer MH, Bruce G, Lanham S, et al. Genetically-programmed, mesenchymal stromal cell-laden & mechanically strong 3D bioprinted scaffolds for bone repair. Journal of controlled release. 2020;325:335-46.
86. Hyde SC, Pringle IA, Abdullah S, Lawton AE, Davies LA, Varathalingam A, et al. CpG-free plasmids confer reduced inflammation and sustained pulmonary gene expression. Nature biotechnology. 2008;26(5):549-51.
87. Takahiko M, Constance LC. Electroporation and RNA interference in the rodent retina in vivo and in vitro. Proceedings of the National Academy of Sciences - PNAS. 2003;101(1):16-22.
88. Hong K, Sherley J, Lauffenburger DA. Methylation of episomal plasmids as a barrier to transient gene expression via a synthetic delivery vector. Biomolecular Engineering. 2001;18(4):185-92.
89. Hsu Patrick D, Lander Eric S, Zhang F. Development and Applications of CRISPR-Cas9 for Genome Engineering. Cell (Cambridge). 2014;157(6):1262-78.
90. Aronovich EL, McIvor RS, Hackett PB. The Sleeping Beauty transposon system: a non-viral vector for gene therapy. Human molecular genetics. 2011;20(R1):R14-R20.
91. Kebriaei P, Izsvák Z, Narayanavari SA, Singh H, Ivics Z. Gene Therapy with the Sleeping Beauty Transposon System. Trends in genetics. 2017;33(11):852-70.
92. Bhatt S, Chalmers R. Targeted DNA transposition in vitro using a dCas9-transposase fusion protein. Nucleic acids research. 2019;47(15):8126-35.
93. Chaikind B, Bessen JL, Thompson DB, Hu JH, Liu DR. A programmable Cas9-serine recombinase fusion protein that operates on DNA sequences in mammalian cells. Nucleic acids research. 2016;44(20):9758-70.
94. Suresh B, Ramakrishna S, Kim H. Cell-Penetrating Peptide-Mediated Delivery of Cas9 Protein and Guide RNA for Genome Editing. Eukaryotic Transcriptional and Post-Transcriptional Gene Expression Regulation. 2016;1507:81-94.
95. Branter J, Dixon J. ATM Gene Delivery Progress Report. 2019 (Unpublished).
96. Foroozandeh P, Aziz AA. Insight into Cellular Uptake and Intracellular Trafficking of Nanoparticles. Nanoscale research letters. 2018;13(1):1-12.
97. Honary S, Zahir F. Effect of Zeta Potential on the Properties of Nano-Drug Delivery Systems - A Review (Part 2). Tropical journal of pharmaceutical research. 2013;12(2).
98. PrestoBlue™ Cell Viability Reagent; https://www.thermofisher.com/order/catalog/product/A13261#/A13261; Thermo Fisher Scientific.
99. DYKDDDDK Tag Monoclonal Antibody (FG4R); https://www.thermofisher.com/antibody/product/DYKDDDDK-Tag-Antibody-clone-FG4R-Monoclonal/MA1-91878; Thermo Fisher Scientific.
100. Paul-Smith MC, Pytel KM, Gelinas J-F, McIntosh J, Pringle I, Davies L, et al. The murine lung as a factory to produce secreted intrapulmonary and circulatory proteins. Gene therapy. 2018;25(5):345-58.
101. Han YH MH, You BR, Park WH. The effect of MG132, a proteasome inhibitor on HeLa cells in relation to cell growth, reactive oxygen species and GSH. Oncology Reports. 2009;22:215-21.
102. Andreatta C, Nahreini P, Hovland AR, Kumar B, Edwards-Prasad J, Prasad KN. Use of Short-Lived Green Fluorescent Protein for the Detection of Proteasome Inhibition. BioTechniques. 2001;30(3):656-60.
103. Lee JH, Choy ML, Ngo L, Foster SS, Paul AM. Histone deacetylase inhibitor induces DNA damage, which normal but not transformed cells can repair. Proceedings of the National Academy of Sciences - PNAS. 2010;107(33):14639-44.
104. Muratori M, Forti G, Baldi E. Comparing flow cytometry and fluorescence microscopy for analyzing human sperm DNA fragmentation by TUNEL labeling. Cytometry Part A. 2008;73A(9):785-7.
105. Immunocytochemistry and immunofluorescence staining protocol; https://www.abcam.com/protocols/immunocytochemistry-immunofluorescence-protocol; Abcam.
106. Swift K, Dubern J. Immunofluorescence (Direct and Indirect). Standard Operating Procedures (2019), Centre for Biomolecular Sciences, University of Nottingham (Unpublished Standard Operating Procedure).

107. Bradbury MWB, Sarna GS. Homeostasis of the ionic composition of the cerebrospinal fluid. Experimental eye research. 1977;25:249-57.
108. Dixon J, Suk J, Prayle A. Brain-penetrating peptide nanoparticles for permanent ATM editing and augmentation. University of Nottingham: Action for A-T; 2015 (Grant Application).
109. Duncan GA, Jung J, Hanes J, Suk JS. The Mucus Barrier to Inhaled Gene Therapy. Molecular therapy. 2016;24(12):2043-53.
110. Kim N, Duncan GA, Hanes J, Suk JS. Barriers to inhaled gene therapy of obstructive lung diseases: A review. Journal of controlled release. 2016;240:465-88.
111. Crater JS, Carrier RL. Barrier Properties of Gastrointestinal Mucus to Nanoparticle Transport: Barrier Properties of Gastrointestinal Mucus to Nanoparticle. Macromolecular bioscience. 2010;10(12):1473-83.
112. Cell Cycle Analysis; https://cancer.wisc.edu/research/wp-content/uploads/2017/08/Flow_TechNotes_Cell-cycle-analysis_20170918.pdf2017; Laboratory UFC.
113. Schuster BS, Ensign LM, Allan DB, Suk JS, Hanes J. Particle tracking in drug and gene delivery research: State-of-the-art applications and methods. Advanced drug delivery reviews. 2015;91:70-91.
114. Dixon J. Non-viral gene therapy for Ataxia telangiectasia (AT). University of Nottingham: AT Children's Project; 2018 (Grant Application).
115. Alton EWFW, Beekman JM, Boyd AC, Brand J, Carlon MS, Connolly MM, et al. Preparation for a first-in-man lentivirus trial in patients with cystic fibrosis. Thorax. 2017;72(2):137-47.
116. Mitomo K, Griesenbach U, Inoue M, Somerton L, Meng C, Akiba E, et al. Toward Gene Therapy for Cystic Fibrosis Using a Lentivirus Pseudotyped With Sendai Virus Envelopes. Molecular therapy. 2010;18(6):1173-82.
117. Ogi T, Walker S, Stiff T, Hobson E, Limsirichaikul S, Carpenter G, et al. Identification of the First ATRIP–Deficient Patient and Novel Mutations in ATR Define a Clinical Spectrum for ATR–ATRIP Seckel Syndrome. PLoS genetics. 2012;8(11):e1002945-e.
118. Chauveau C, Rowell J, Ferreiro A. A Rising Titan: TTN Review and Mutation Update. Human mutation. 2014;35(9):1046-59.